1976

Hydraulic ram effect on composite fuel entry walls.

Duva, Alfred Nicholas

HYDRAULIC RAM EFFECT ON COMPOSITE FUEL CELL ENTRY WALLS

Alfred Nicholas Duva

NAVAL POSTGRADUATE SCHOOL
Monterey, California

THESIS

HYDRAULIC RAM EFFECT
ON
COMPOSITE FUEL CELL ENTRY WALLS

by

Alfred Nicholas Duva Jr.

March 1976

Thesis Advisor: R. E. Ball

Approved for public release; distribution unlimited.

SECURITY CLASSIFICATION OF THIS PAGE (When Data Entered)

REPORT DOCUMENTATION PAGE

READ INSTRUCTIONS BEFORE COMPLETING FORM

1. REPORT NUMBER	2. GOVT ACCESSION NO. / 3. RECIPIENT'S CATALOG NUMBER
4. TITLE (and Subtitle): Hydraulic Ram Effect on Composite Fuel Cell Entry Walls	5. TYPE OF REPORT & PERIOD COVERED: Master's Thesis, March 1976
	6. PERFORMING ORG. REPORT NUMBER
7. AUTHOR(s): Alfred Nicholas Duva Jr.	8. CONTRACT OR GRANT NUMBER(s)
9. PERFORMING ORGANIZATION NAME AND ADDRESS: Naval Postgraduate School, Monterey, California 93940	10. PROGRAM ELEMENT, PROJECT, TASK AREA & WORK UNIT NUMBERS
11. CONTROLLING OFFICE NAME AND ADDRESS: Naval Postgraduate School, Monterey, California 93940	12. REPORT DATE: March 1976
	13. NUMBER OF PAGES: 76
14. MONITORING AGENCY NAME & ADDRESS(if different from Controlling Office): Naval Postgraduate School, Monterey, California 93940	15. SECURITY CLASS. (of this report): Unclassified
	15a. DECLASSIFICATION/DOWNGRADING SCHEDULE

16. DISTRIBUTION STATEMENT (of this Report)

** Approved for public release; distribution unlimited.

17. DISTRIBUTION STATEMENT (of the abstract entered in Block 20, if different from Report)

18. SUPPLEMENTARY NOTES

19. KEY WORDS (Continue on reverse side if necessary and identify by block number)

20. ABSTRACT (Continue on reverse side if necessary and identify by block number)

Catastrophic failure of a partially filled aircraft fuel cell due to impact and penetration by a high speed projectile often occurs due to a phenomenon known as hydraulic ram. The structural response of the fuel tank walls to hydraulic ram should be of vital concern to the designers of aircraft fuel cells. Considerable research has been conducted to determine the effects of hydraulic ram on metallic fuel cells, but very little attention

DD FORM 1 JAN 73 1473 EDITION OF 1 NOV 65 IS OBSOLETE
S/N 0102-014-6601 |
(Page 1)

SECURITY CLASSIFICATION OF THIS PAGE (When Data Entered)

has been given to fuel cells made with the new advanced composite materials. The purpose of this research is to examine the various effects of hydraulic ram on a graphite/epoxy wall when subjected to penetration by a .222 caliber projectile. Eight hydraulic ram tests are made on a clamped 11-inch square plate 0.067 inches thick at projectile velocities between 2600 and 2800 fps. The engineering properties of the laminate are determined both analytically and experimentally. The low velocity shots caused only slight damage to the plate. At the higher velocities, the hydraulic ram caused considerable damage, including total severance of the plate from its clamped support over much of the outer perimeter. The results of this research illustrate the importance of the method of attachment of the composite wall at its boundaries.

Hydraulic Ram Effect on Composite Fuel Cell Entry Walls

by

Alfred Nicholas Duva Jr.
Lieutenant Commander, United States Navy
B.S., Fairleigh Dickinson University, 1965

Submitted in partial fulfillment of the requirements for the degree of

MASTER OF SCIENCE IN AERONAUTICAL ENGINEERING

from the

NAVAL POSTGRADUATE SCHOOL
March 1976

ABSTRACT

Catastrophic failure of a partially filled aircraft fuel cell due to impact and penetration by a high speed projectile often occurs due to a phenomenon known as hydraulic ram. The structural response of the fuel tank walls to hydraulic ram should be of vital concern to the designers of aircraft fuel cells. Considerable research has been conducted to determine the effects of hydraulic ram on metallic fuel cells, but very little attention has been given to fuel cells made with the new advanced composite materials. The purpose of this research is to examine the various effects of hydraulic ram on a graphite/epoxy wall when subjected to penetration by a .222 caliber projectile. Eight hydraulic ram tests are made on a clamped 11-inch square plate 0.067 inches thick at projectile velocities between 2600 and 2800 fps. The engineering properties of the laminate are determined both analytically and experimentally. The low velocity shots caused only slight damage to the plate. At the higher velocities, the hydraulic ram caused considerable damage, including total severance of the plate from its clamped support over much of the outer perimeter. The results of this research illustrate the importance of the method of attachment of the composite wall at its boundaries.

TABLE OF CONTENTS

LIST OF FIGURES

LIST OF TABLES

LIST OF SYMBOLS

A_{ij} - extensional rigidities

B_{ij} - coupling matrix

C_{ij} - elements of the stiffness matrix

D_{ij} - flexural rigidities

E - Young's modulus

G - shear modulus

h - lamina thickness

M - moment

N - force

Q_{ij} - reduced stiffness matrix

$\bar{Q}_{ij}$ - transformed reduced stiffness matrix

t - laminate thickness

u,v,w - components of the displacement vector

α, β - arbitrary angles

ε - strain

ν - Poisson's ratio

ξ, η - 45° orientation from the laminate axis

θ - angular orientation of a lamina in a laminate

λ - constant

ρ - mass/unit area

σ - stress

ω - frequency

$\sum$ - summation

SUBSCRIPTS

i, j - 1, 2, 3

k - k^{th} position in sequence

x, y, z- general coordinate system

1 - longitudinal axis of the laminate

2 - transverse axis of the laminate

SUPERSCRIPTS

(k) - k^{th} ply or lamina

I. INTRODUCTION

The composite lamination concept provides greatly increased opportunities for tailoring structures and/or materials to meet systems of forces and changing environments. Achieving this goal requires both new techniques in design and manufacture and the accumulation of vast amounts of information on the properties of a whole new family of materials. The technology of composites is actually in its infancy; typical of most new technologies, applications based on purely empirical results have far outpaced the theoretical developments. Analytical analyses that are representative of the current state of the art have been attempted, but many theoretical investigations are still needed in certain areas.

Composites, such as boron-epoxy and graphite-epoxy, have been successfully employed as structural materials in aircraft, missiles, and space vehicles, and have satisfactorily demonstrated their performance through extensive ground and flight testing. In general, advanced composites have tremendous advantages over metals in applications requiring high strength, high stiffness, and low weight. However, in applications where impact of foreign objects is a design consideration, the advantages inherent in composites are overshadowed by their poor response to impact loading. A better understanding of this problem is needed so that the survivability of composites to impact loading can be increased.

Ballistic impact and penetration into fuel cells by small arms projectiles and missile fragments is a significant factor in generating catastrophic failure of military aircraft components. When a high-velocity projectile penetrates a fuel cell, high pressures can be generated in the contained liquid as a result of the deceleration of the projectile by the liquid. These pressures act on the fuel cell walls and can cause catastrophic failure of the cell's structural components. The interaction of the fluid-containing cell with the penetrating projectile is referred to as hydraulic ram.

This research is directed toward increasing the survivability of a composite-structure aircraft fuel cell subjected to a high energy ballistic impact and penetration. The laminated composite plates tested were designed and fabricated by the Naval Weapons Center, China Lake. Each of the eight graphite/epoxy test plates were of antisymmetric angle-ply design with $0/\pm45/90/0/\pm45/90/0$ degree 9-ply fiber orientation. The laminate engineering properties are computed analytically from the generalized Hooke's Law and compared to those determined experimentally with the use of strain gages.

Several composite plates were used as the entry wall of a simulated fuel cell and penetrated by a .222 caliber projectile at velocities between 2600 and 2800 fps. The degree of damage incurred with/without hydraulic ram effect was visually and microscopically examined, and the possibility of measuring the amount of laminate damage as a function of the fundamental natural frequency of the plate was investigated.

II. APPLICATIONS OF COMPOSITE MATERIALS

A. COMMERCIAL AIRCRAFT

The aircraft industry has taken an intense interest in advanced fibrous reinforced composites. Proper use of these new materials offers potential for reducing the weight of aircraft structural components by as much as fifty percent and, therefore, increasing the productivity of commercial aircraft. Basic structural elements such as skins, spars, stiffeners and frames offer the most potential for cost effective weight reduction. Components such as control surfaces, while advancing the state of the art, offer less potential. For unidirectional loading, advanced composites provide a significant weight reduction, with the added advantage of being relatively easy to fabricate, analyze, and design. As a result, initial commercial applications of advanced composites have been in beam flanges, columns, longerons, stringers and frames, with the incorporation of advanced structural concepts such as honeycomb sandwich skins to provide the additional structural stability required.

An initial step toward the use of advanced composites in commercial aircraft structures was the design, analysis, fabrication, and test of an aircraft floor beam with boron-epoxy flanges and a titanium-aluminum honeycomb web. This beam was designed to replace the Boeing 707 web-stiffened aluminum floor beam. While the quantity of boron filament

contained in the beam was only about 20 percent of the total beam weight of 9 pounds, it was positioned and utilized so as to take maximum advantage of the advanced composite properties. Although far exceeding the structural performance of the original aluminum beam, a cost effectiveness study indicated that weight was saved at a cost of $107 per pound for this application of boron composites, assuming a boron filament cost of $150 per pound.

The feasibility of stiffening compression panels with boron-epoxy composite was demonstrated by the design, analysis, fabrication, and test of a composite compression panel. The composite panel proved to be 53 percent lighter than an equivalent conventional all titanium skin and stringer design. The load carrying capacity chosen for design purposes was that which is typically sustained by the upper surface of a Boeing 707 wing panel at mid-span. A cost study revealed that this particular application saved weight at a cost of $52 per pound saved. This put it well within the range of being cost effective for potential use on subsonic commercial aircraft.

Before composites can be extensively used in future commercial aircraft their performance under in-service environments must be determined. In addition to specimen testing to determine the effect of extremes in environment, in-service evaluations of simple structural components should be performed. Preferably, these components should be readily installed to facilitate flight testing and should not be protected from normal in-service damage. Examples of this kind of structure

are control surfaces, such as foreflaps and spoilers. The conventional Boeing 707 rib stiffened aluminum foreflap has been redesigned using advanced composites. Fabrication, static, fatigue and flight tests have been successfully completed. Cross-plied graphite-epoxy skins were used to replace the existing aluminum skins and to resist torsional loads on the Boeing 737 flight spoiler. Because these components are relatively small and lightly loaded, have problems with attachments, and have minimum gage, they offer only marginal potential for cost effective weight savings. However, due to the extremes of environment seen by these components, they will play a vital role in the rapid development and acceptance of advanced composites for use on commercial aircraft by providing considerable service experience in the near future.

On many structural components which fall below expected stiffness or strength requirements advanced composites can be used for a least-added-weight fix. For example, one third of a pound of boron composite was used to stiffen a ceiling panel to meet minimum design requirements, whereas 1.5 pounds of fiberglass would have been required to meet the same requirements. During verification testing of a proposed aircraft fiberglass seat, it was determined that the static defection of the seat under service loading exceeded the maximum amount allowed. The addition of just one pound of boron composite was shown to be sufficient to stiffen the seat, while 4.5 pounds of fiberglass would have been required to accomplish the same result.

Future commercial aircraft designs must incorporate the best combination of material and design concepts in order to meet increased demands for high performance. A new class of materials having the potential for reducing total structural airframe weight by a significant amount, without sacrificing reliability or structural integrity, has now been made available to the aircraft designer - the advanced composite.

B. MILITARY AIRCRAFT

Composites have been used in the design of military aircraft for more than twenty-five years (Figure II.B.1). The bulk of this use has been glass fiber reinforced plastics, providing both improved structural efficiency and lower cost. The advent of the high modulus composites (boron and graphite) has recently led to their use in highly loaded, stiffness critical wings and control surfaces, as well as for other structural components. The initial composite material development was made in the 1930's by Owen-Corning with the commercial production of glass fibers. Glass fiber reinforced plastic (GFRP) materials were first developed and designed for airframe structures at the U. S. Air Force Wright Air Development Center in 1943. The aft fuselage honeycomb skin of the Vultee BT-16 was the first such structure fabricated. The construction was a balsa wood core with skins consisting of polyester resin impregnated with glass fibers. The next major step was taken at Wright Field with the fabrication of the outer wing

Figure II.B.1 - Chronology of Composite Usage

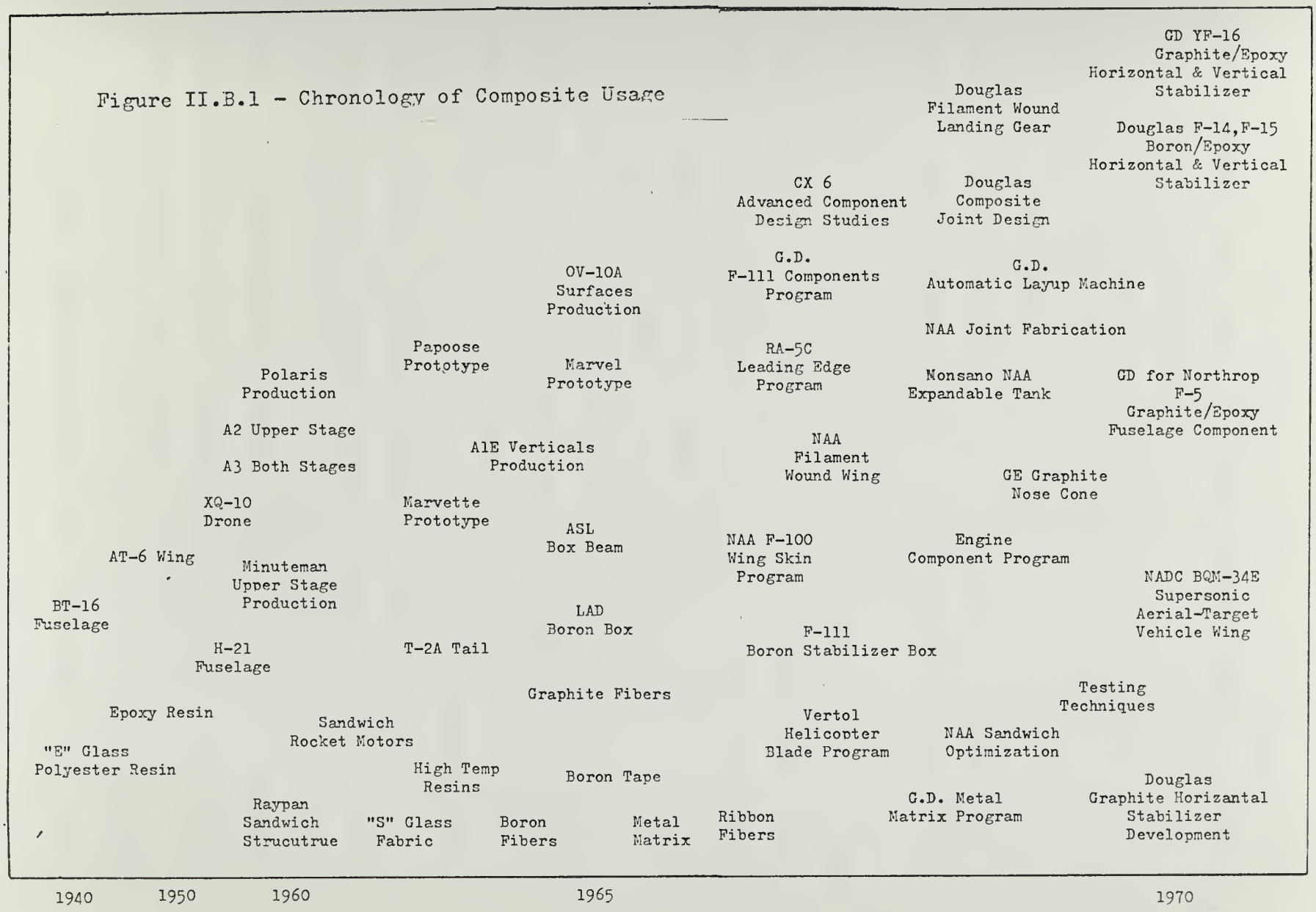

panels for the AT-6 airplane. However, many problems still remained with the use of polyester resins, such as weathering and temperature properties.

With the synthesis of epoxy resins in the 1950's, aircraft engineers were provided with a reinforced plastic system of highly improved weathering ability. 1959 brought the development of a Fairchild surveillance drone system using GFRP. The significant contribution of this program was the use of the GFRP structure as an integral fuel tank.

During the 1950's many applications were found for GFRP, especially in the nonstructural areas of operational aircraft. Today reinforced plastics are being used to an even greater extent. However, the role of GFRP remains one of a secondary or nonstructural nature in the general case.

Early in 1963 North American Aviation, under contract to the Navy's Aeronautical Structures Laboratory, Philadelphia, Pa., undertook a GFRP structure research and development program. The purpose of this program was to evaluate the static strength, fatigue, and weight characteristics of a typical military aircraft component using available glass fiber reinforced plastic technology. Supplementary programs were also conducted to provide insight into other design considerations such as repairability, vulnerability, cost, noise attenuation, performance, and corrosion.

Also in the early 1960's came the production of Polaris and Minute Man missile systems, the first major structural application of GFRP to military aerospace systems. The ideal

application of the high tensile strength of glass fiber were in the rocket motor cases. Substantial performance gains were realized on these programs over the conventional metal cases. In mid 1960's the Army sponsored a program with Mississippi State University for the investigation of a high lift low drag aircraft configuration. The result of this program was the fabrication of two all GFRP aircraft (Marvellet and Marvel prototypes). During this same time period the Grumman Aircraft Corp. initiated a production program for the vertical stabilizers on the A1E aircraft. Although the requirement was for electronic purposes, it did require the application of GFRP to the primary structure of the vertical stabilizer and became the first production application.

It was also in the mid 1960's that boron fibers became available to the industry in limited quantities, and the first advanced filamentary composite hardware programs were begun. The two major boron application programs were the General Dynamics F-111 Horizontal Stabilizer Program and the Boeing Vertol Helicopter Blade Program. Both of these programs involved the extensive development of design and fabrication techniques with boron filamentary composites. Substantial advantages of the application of boron composites to the military air vehicle system have been realized in both programs. The development and manufacturing techniques also proved very important at this time for the continuing progress of filamentary composites. A contract to develop a production tape lay-up machine was awarded to General Dynamics, while a

contract to demonstrate the application of filament winding to an aircraft lifting surface structure was awarded to North American Aviation. Both programs, successful in meeting their objectives, established a new basis for the fabrication of filamentary composite structures.

The Air Force has entered into many development contracts directed toward re-entry vehicles, aircraft power plants, aircraft wing and fuselage structures, and all types of structural applications in military aircraft. The great interest shown by the Air Force and participating contractors has culminated in the application of filamentary composites to systems such as the F14, F15, and B1.

C. GENERAL ADVANTAGES

Many advantages will be gained through the use of fiber reinforced plastics in primary airframe structures. Inherent "fail-safe" characteristics for high load-carrying capability after damage are provided by multicontinuous fiber load paths and bonded joints.

Good notch insensitivity with attendant low crack propagation leads to excellent fatigue properties of filamentary composite materials. On the basis of fatigue life to weight ratio, filamentary composites show as much as 100 percent improvement over titanium, which is the best of the metals in fatigue.

The fact that the structure can be made of a minimum number of large, one-piece subassemblies is another advantage. This reduction of parts manifests itself by lowering tooling costs,

fabrication costs, handling costs, and, finally, greater reliability through reduction of the number of points and discontinuities in the structure.

Composites exhibit high structural damping properties (especially in sandwich construction), greatly reducing vibration and noise transmission.

Composites also provide increased flight performance due to reduced parasite drag coefficient of the smooth skin finish. The work at Mississippi State University under the Army Marvellet Program demonstrated reductions of as much as 40 percent in the parasite drag or approximately 15 to 20 percent of the total drag.

Minor field repairs are facilitated by the lack of crack propagation, and such repairs can be limited to nonstructural patches sufficient to maintain a smooth aerodynamic surface.

Reinforced plastic materials provide a capability for both active and passive radar nonreflective systems. The use of such systems in the basic design of military aircraft can reduce the detection range for aircraft substantially. The capability of a GFRP lifting surface to pass radar energy through the surface reduces the detection range by 50 percent.

Another example is the case of the high speed air superiority fighter, where drag is of prime interest to the performance. One of the parameters determining aircraft drag is the wing thickness. The high stiffness weight and strength weight ratios of advanced composites allow the designers to consider reducing the wing thickness without paying severe weight

penalties. Maintaining an equal weight to the conventional metal aircraft, the thickness can be reduced significantly to produce a lower drag aircraft. Through these types of design trade offs and greater structure flexibility, significant changes in aircraft configurations can be expected in the future.

D. HYDRAULIC RAM STUDIES

Catastrophic failure of a liquid containing fuel cell due to impact by a high speed projectile is often caused by a phenomenon known as hydraulic ram. The structural response to hydraulic ram should be of vital concern to the designers of advanced composite aircraft fuel cells. In order to prevent or reduce the amount of damage, the failure mechanisms of the fuel cells must be understood.

Projectiles that penetrate liquid-containing cells cause structural damage many times more severe than that incurred by impact with empty cells. The penetration of the projectile through the liquid in the cell causes an energy transfer from the projectile to the fluid and the cell walls. The initial phase of the transfer occurs when the projectile penetrates the entry wall and compresses the liquid near the entry point, resulting in extremely high fluid pressures of the order 10^5 pounds per square inch. These pressures produce a shock wave which propagates spherically outward from the entry point. Generally, the shock attenuates rapidly and becomes too weak

to cause any damage to the side or exit walls of the fuel cell. However, it can contribute to outward petaling of the entrance wall in the vicinity of the entry point.

As the projectile moves through the liquid it must displace the liquid from its path. A large radial velocity is thus imparted to the liquid, and, as a result, the liquid moves away from the projectile path eventually creating a cavity. Pressures during the penetration or drag phase are of the order 10^3 pounds per square inch, and last considerably longer than those produced by the shock wave. The cavity growth is eventually contained by existing liquid pressures causing the onset of cavity collapse. Inside the cavity are fluid vapors and trapped air which entered during wall penetration. As the cavity collapses, this air is compressed to a high pressure resulting in re-expansion of the cavity. Expansion and collapse repeat several times before all the stored energy is dissipated. As the liquid attempts to regain its undisturbed equilibrium condition, the cavity will oscillate. The accompanying pressures will pump liquid from the cell and may be sufficient to cause additional damage to fuel cell components.

With the introduction of advanced composite materials to aircraft design, the effect of hydraulic ram on fuel cell structural components is of increasing concern. The major aircraft corporations, including Northrop, General Dynamics, Boeing, and McDonnell Douglas, have been contracted by government agencies to conduct studies of this potential problem area.

III. TEST FACILITIES AND SPECIMENS

A. TEST SPECIMENS

The composite test specimens were manufactured from NARMCO 5208/T 300 graphite/epoxy at the Propulsion Development Department, Naval Weapons Center, China Lake. Each 9-ply plate was 0/±45/90/0/±45/90/0 degree fiber orientation as shown.

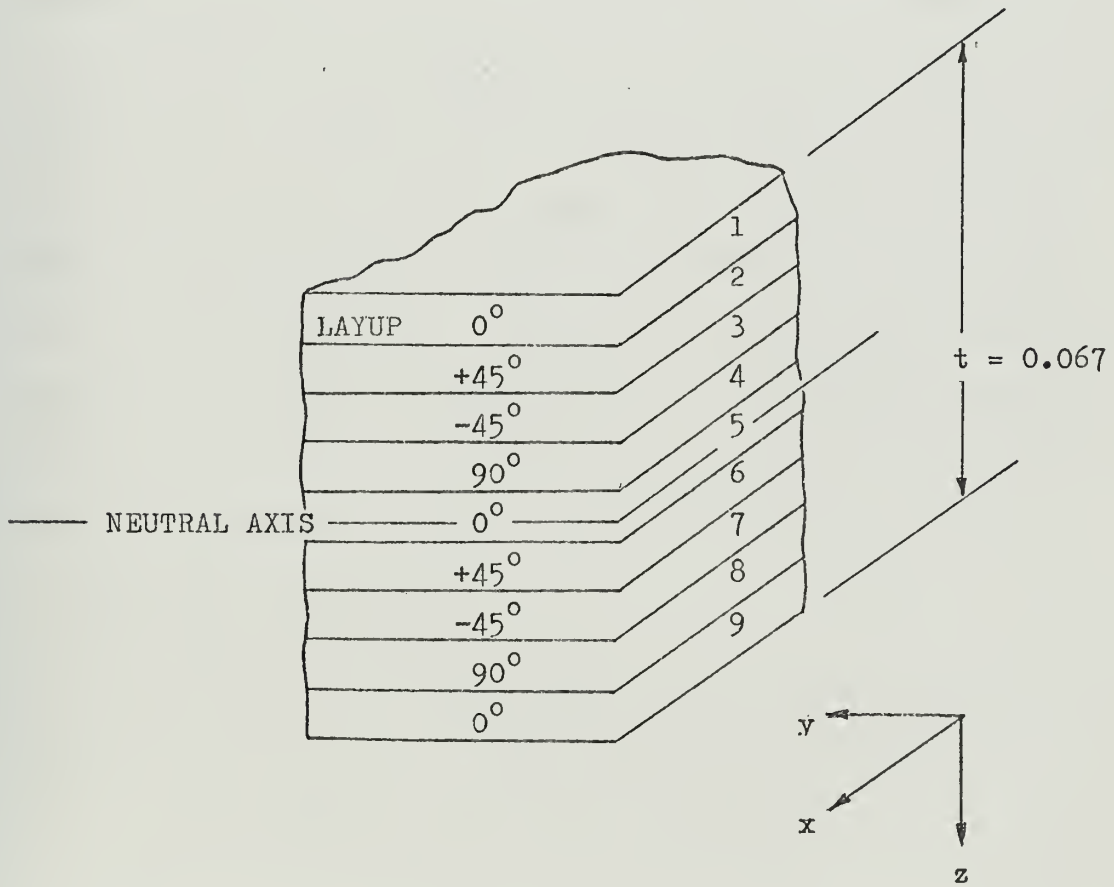

FIGURE III.A.1 - Test Laminate

The dimensions of antisymmetric angle-ply test laminates were 12 by 12 by 0.067 inches. Visual examination of the test plates revealed overall warping and considerable delamination. This condition, directly effecting the strength and stiffness of the laminate, may be attributed to an improper curing process.

B. LAMINATE STIFFNESS PROPERTIES

The equipment setup for testing composite laminates in tension is shown in Figure III.B.1. Each of three 1.5 by 9.5 by 0.067-inch specimens were instrumented with two pairs of SR-4 type biaxial strain gages mounted on the front and back faces of each specimen, as seen in Figure III.B.2. All specimens were loaded in 250-lb increments in a 300,000-lb Riehle Testing Machine. The strain gages were electrically connected to a Baldwin-Lima-Hamilton Channel Switching and Balancing Unit which in turn was connected to a SR-4 Portable Strain Indicator (type N).

C. HYDRAULIC RAM TESTS

The hydraulic ram test system is designed to simulate the response of a composite entry wall of an aircraft fuel cell due to a high energy ballistic penetrator. A down range view of the ballistic range shown in Figure III.C.1 displays the positioning of the basic equipment components. These components are shown in detail in Figure III.C.2.

The rifle mounting system, shown in Figure III.C.3, includes the rifle mount and its rigid, adjustable stand. A .222 caliber

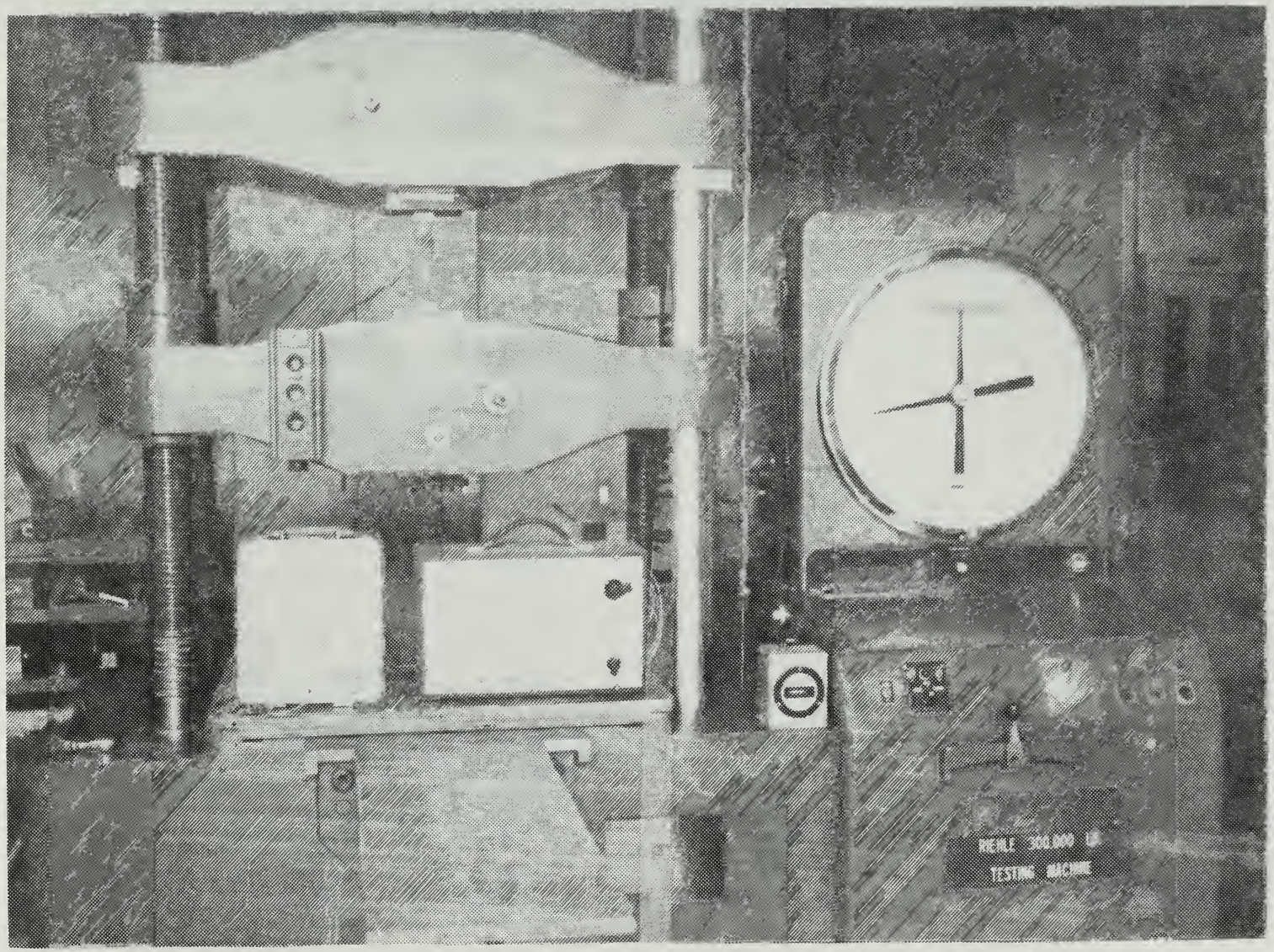

Figure III.B.1 - Stress-Strain Measurement Equipment

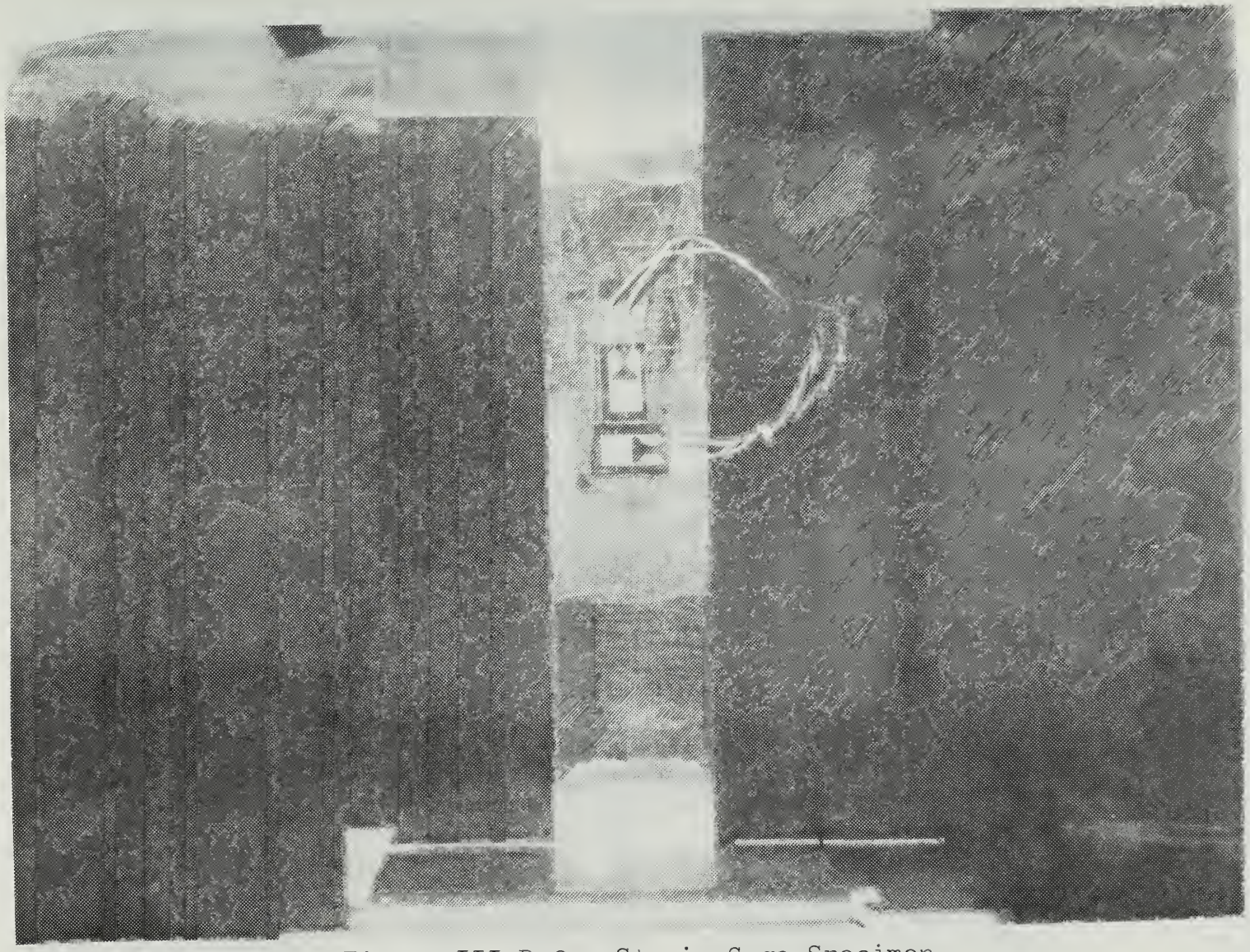

Figure III.B.2 - Strain Gage Specimen

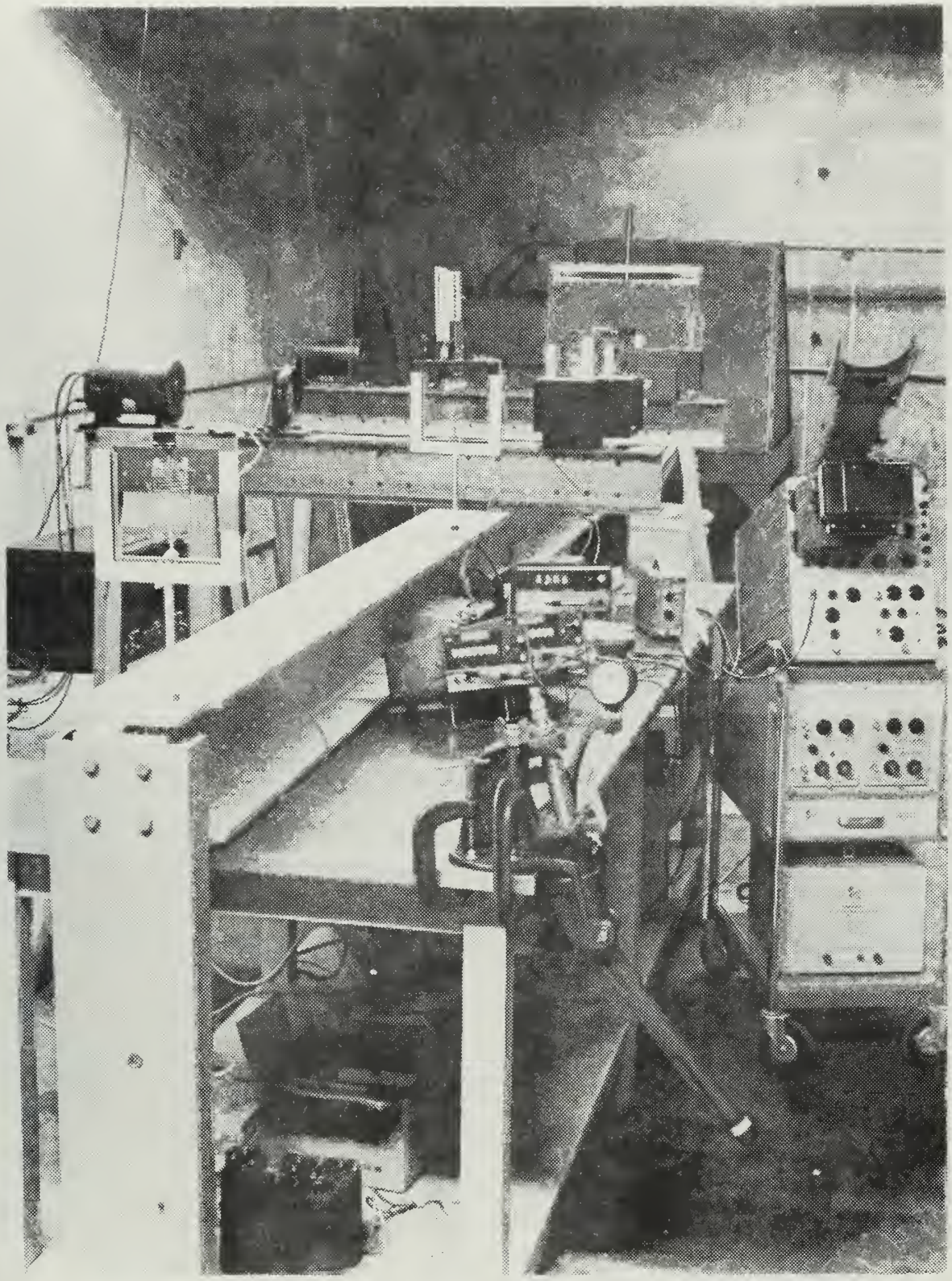

Figure III.C.1 - Ballistic Range

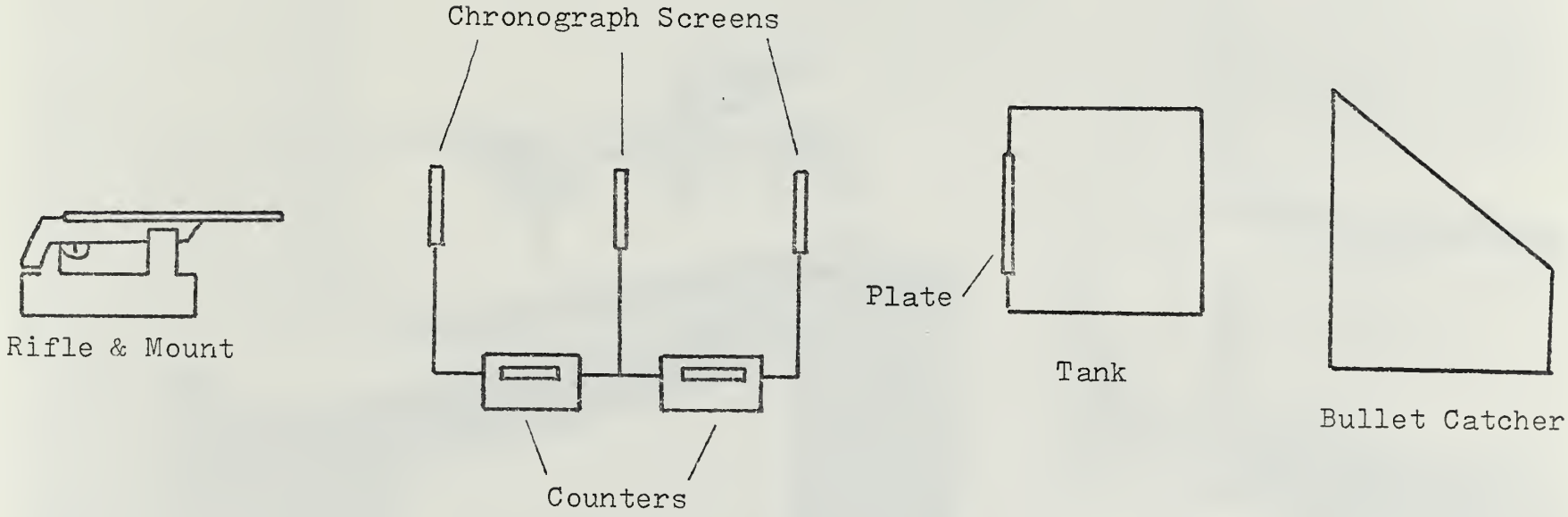

Figure III.C.2 - Basic Components

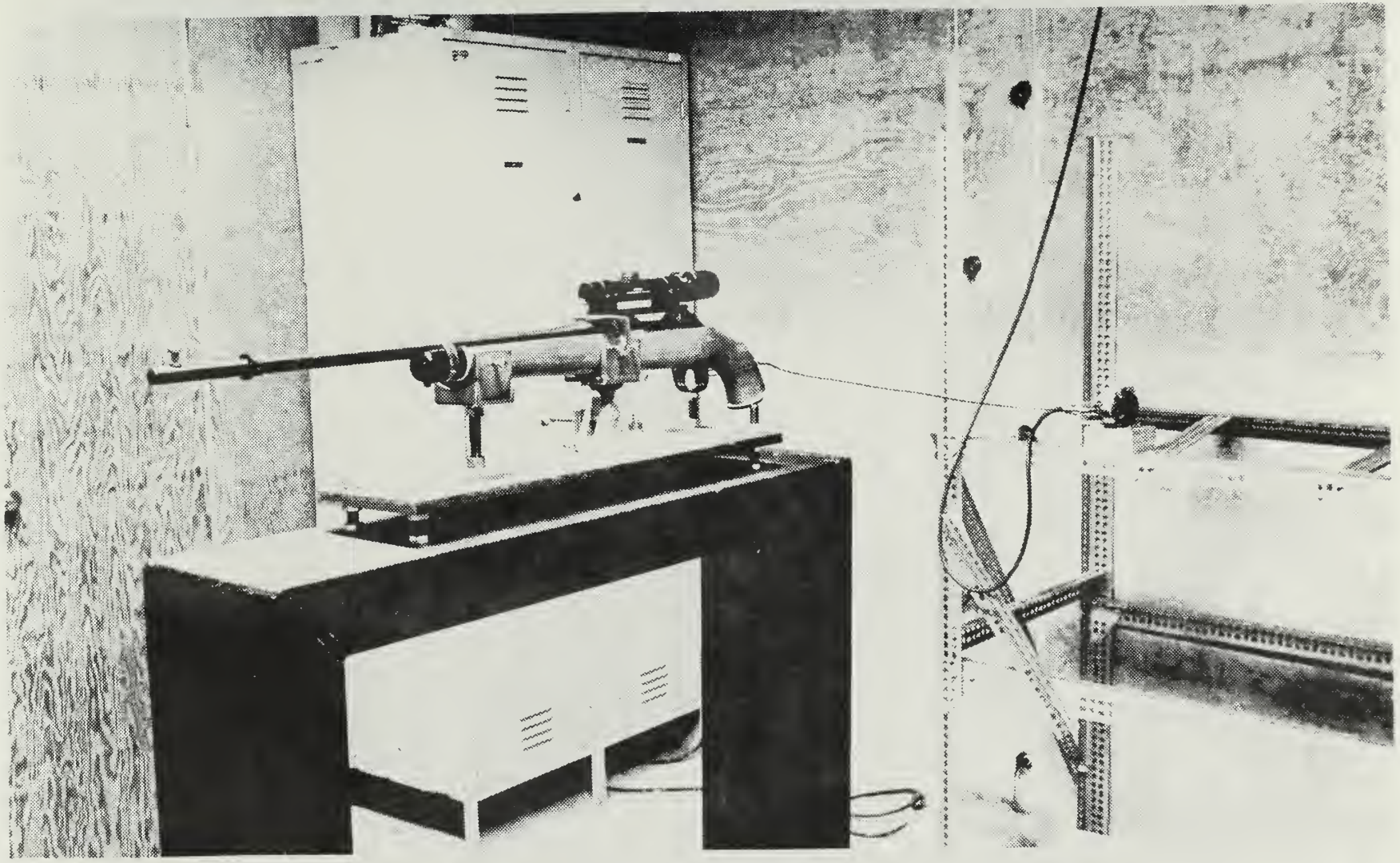

Figure III.C.3 - Rifle Mount/Stand

Remington rifle was used to fire the projectile with the parameters described in Table III.C.1. The projectile velocity was measured by a system of Avtron No. A914T333 Chronograph Screens, mounted six feet apart, electrically connected to two Monsanto Model 101B Counter-Timers. Across each screen was a five volt D.C. signal, shorted to ground. As the projectile penetrated each individual screen, breaking the circuit, start and stop pulses activated the counters. The counters provided the necessary time interval required to predict the average impact velocity at the test cell entry wall.

The simulated fuel cell was the 19-inch cubical tank shown in Figure III.C.4. The 19-inch tank does not represent typical fuel tank dimensions; this size was selected in order to minimize the effects of reflections from the other walls. The base and vertical sides parallel to the projectile flight path were constructed of 0.09-inch 7075-T6 aluminum welded to a 0.75-by 3-inch aluminum frame. The entry and exit walls were bolted to the inside of 1 inch thick aluminum wall supports with a 15.75-inch square and a circular 15-inch diameter cutout, respectively. A 0.09-inch 7075-T6 aluminum plate was bolted to the exit wall support covering the circular cutout, and similarly, a 0.16-inch 7075-T6 plate was bolted to the entry wall support.

An 11-inch square cutout centered on the 0.16-inch entry wall plate was made. The 12-inch square graphite/epoxy test plate was sandwiched between the 0.16-inch front plate and an

TABLE III.C.1

Projectile Parameters

Caliber	.222 Remington	.222 Remington
Impact Velocity (ft/sec)	2500	2900
Projectile Mass (lb)	6.43×10^{-3}	6.43×10^{-3}
Impact Energy (in-lb)	7493	10,072

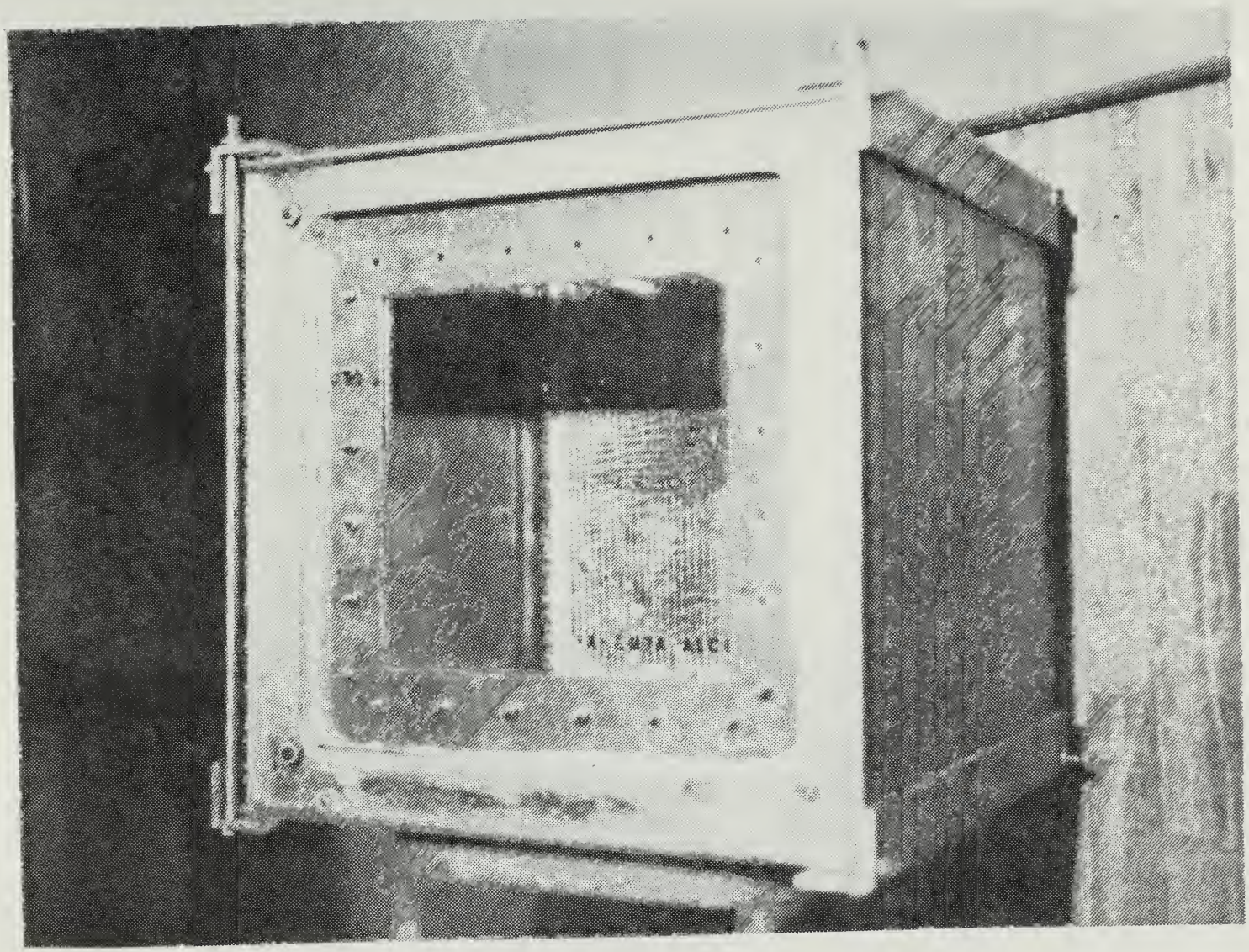

Figure III.C.4 - Test Cell

11-inch square frame 0.16-inch thick. The entire assembly was bolted together outside the perimeter of the graphite/epoxy plate, forming a friction clamped boundary condition. The bolts were positioned approximately 2.5 inches apart. The result was an 11-inch square graphite/epoxy plate entry window shown in Figure III.C.5. The tank was then filled with water, and the top was left open.

A bullet catcher, shown in Figure III.C.6, was used as a safety precaution to prevent possible projectile ricochets. However, due to the limited impact energy levels tested, the projectiles were unable to penetrate the exit wall.

D. VIBRATION TESTS

The system used to determine the natural frequencies of the composite plate specimens is shown in Figures III.D.1 - 2. The Ling Electronics Model CP-3/4-D Amplifier is an electronic power supply capable of supplying a 3-kva power output. The unit is designed for vibration testing applications in the 5 to 10,000 Hz frequency range. This amplifier amplifies sine wave signals in a variable audio frequency and amplitude range, up to the full rated capacity of the associated shaker equipment.

The composite of the model CP-3/4-D amplifier include the Ling Electronics Model S-11 Servo System and a Calidyne Model 219 Vibration Exciter (shaker). The servo system accurately regulates the vibration level at the shaker by holding displacement or acceleration constant as frequency or other

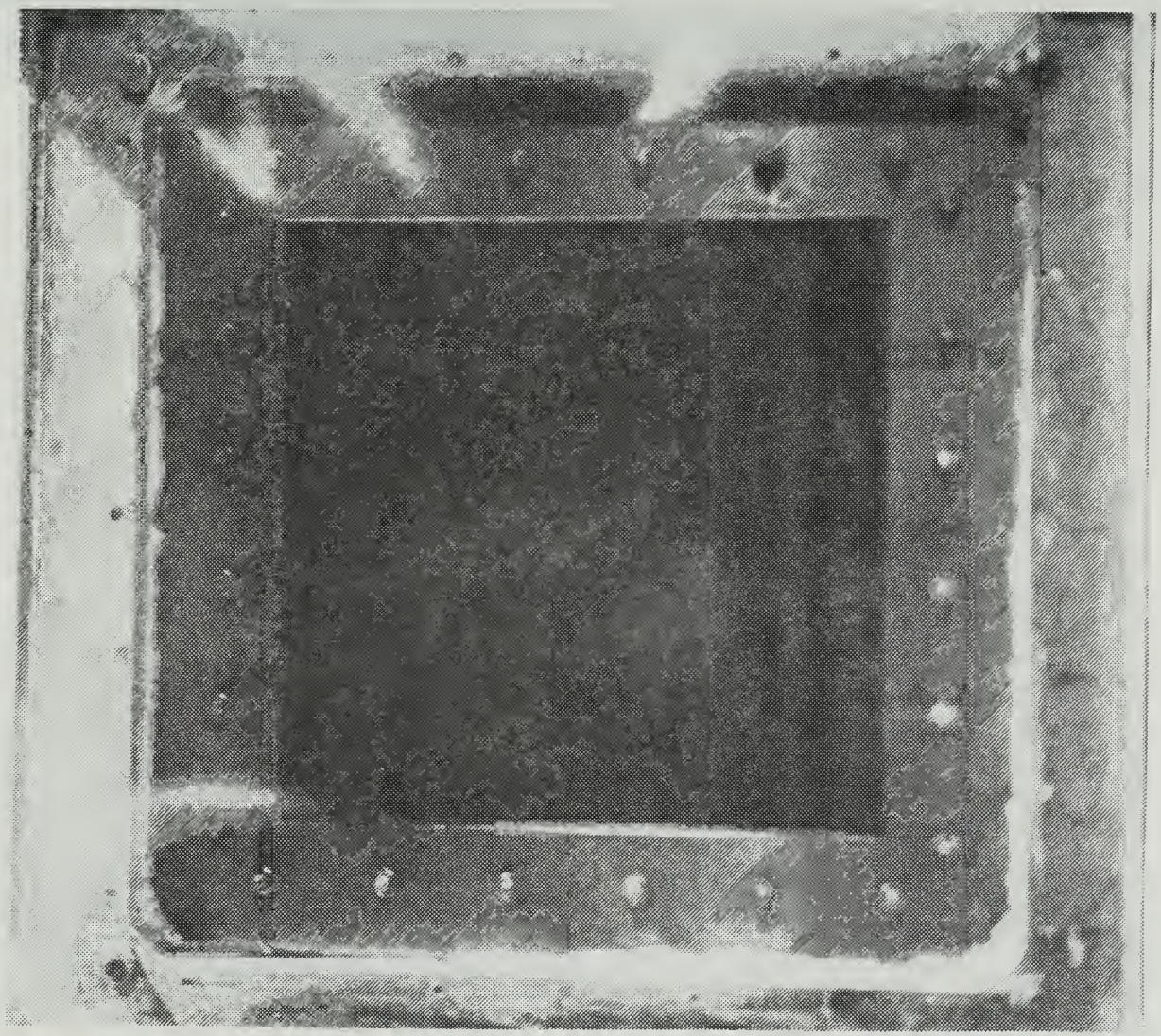

Figure III.C.5 - Graphite/Epoxy Entry Window

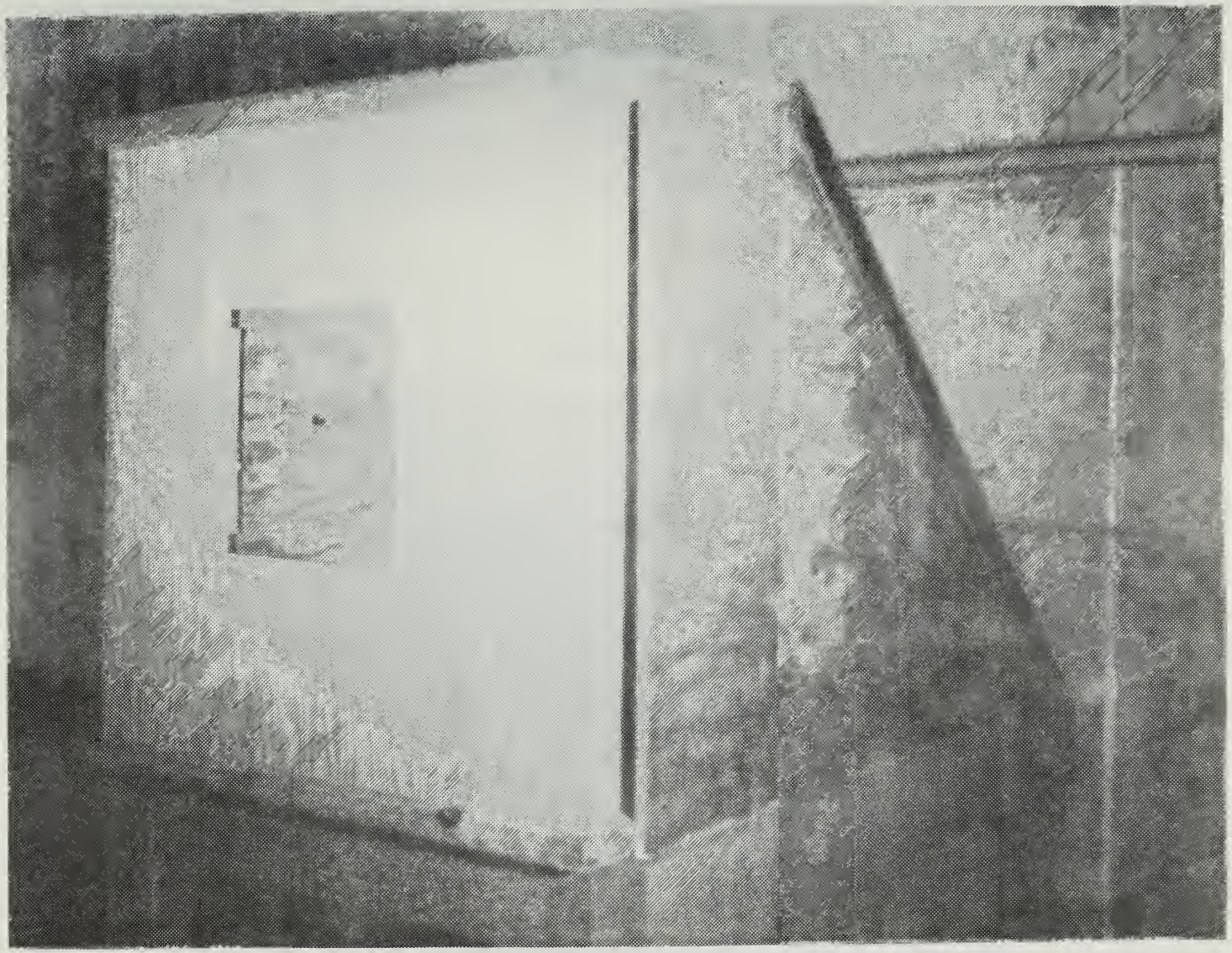

Figure III.C.6 - Bullet Catcher

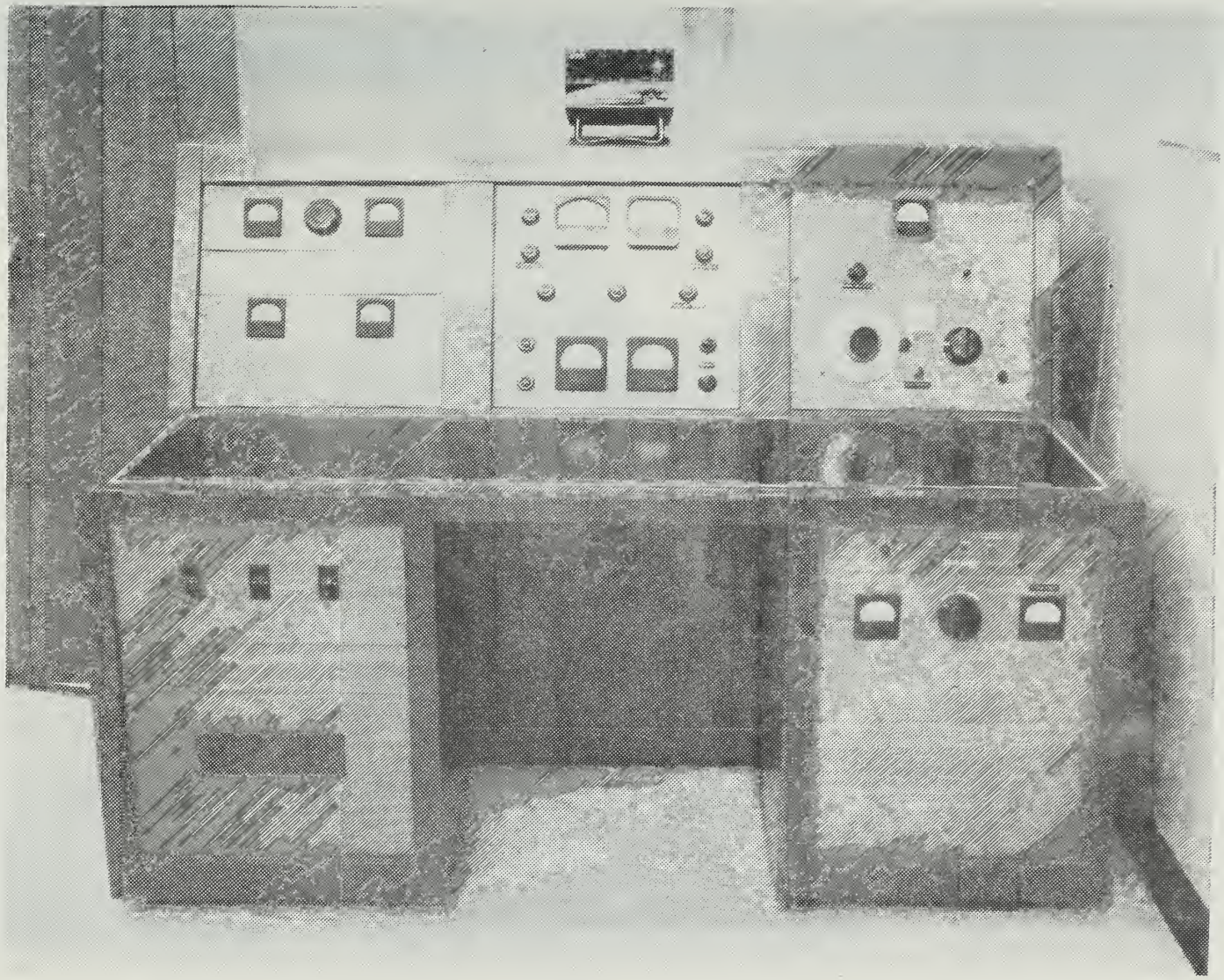

Figure III.D.1 - Model CP-3/4-D Amplifier/Components

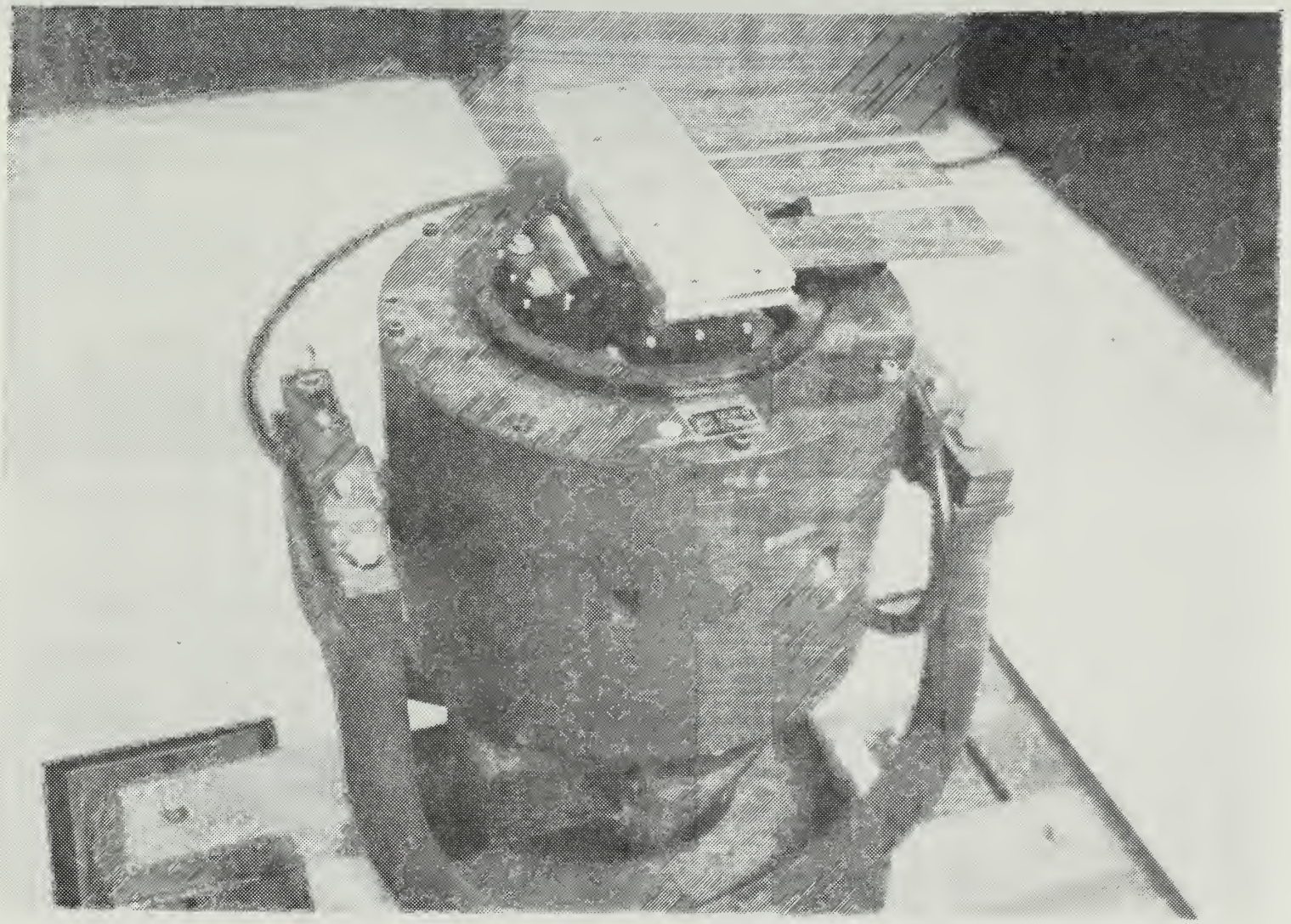

Figure III.D.2 - Shaker Table

parameters are varied in the vibration testing system. The natural frequencies of the structure are determined by varying the frequency at which the structure is shaken. Any frequency at which the response of the structure is noticeably pronounced is a natural frequency.

E. MICROSCOPIC EXAMINATION

Generally, a composite material can be described as a material with several distinct phases present. Normally, the composite consists of a reinforcing material (fiber, whisker) supported in a binder or matrix material. The reinforcing material is the main load carrying medium in the material, and the matrix serves as a carrier, protector and load-splicing medium around the reinforcement. However, the load is usually applied mainly to the matrix, and so it must be transferred to the fiber through adhesion or friction at the matrix-fiber interface. This gives rise to complex stress and strain distributions, with length scale of the order of the fiber diameter, in both the fiber and matrix. Obviously in subjects such as elasticity, plasticity and viscoelasticity, it is helpful to have at least a qualitative appreciation of material behavior at the microscopic level in order to formulate a macroscopic theory.

The Stereoscan S4-10 Scanning Electron Microscope shown in Figure III.E.1 enables the microtopography of solid-bulk specimens to be directly examined and photographed with a minimum of preparation. Its design is based on principles

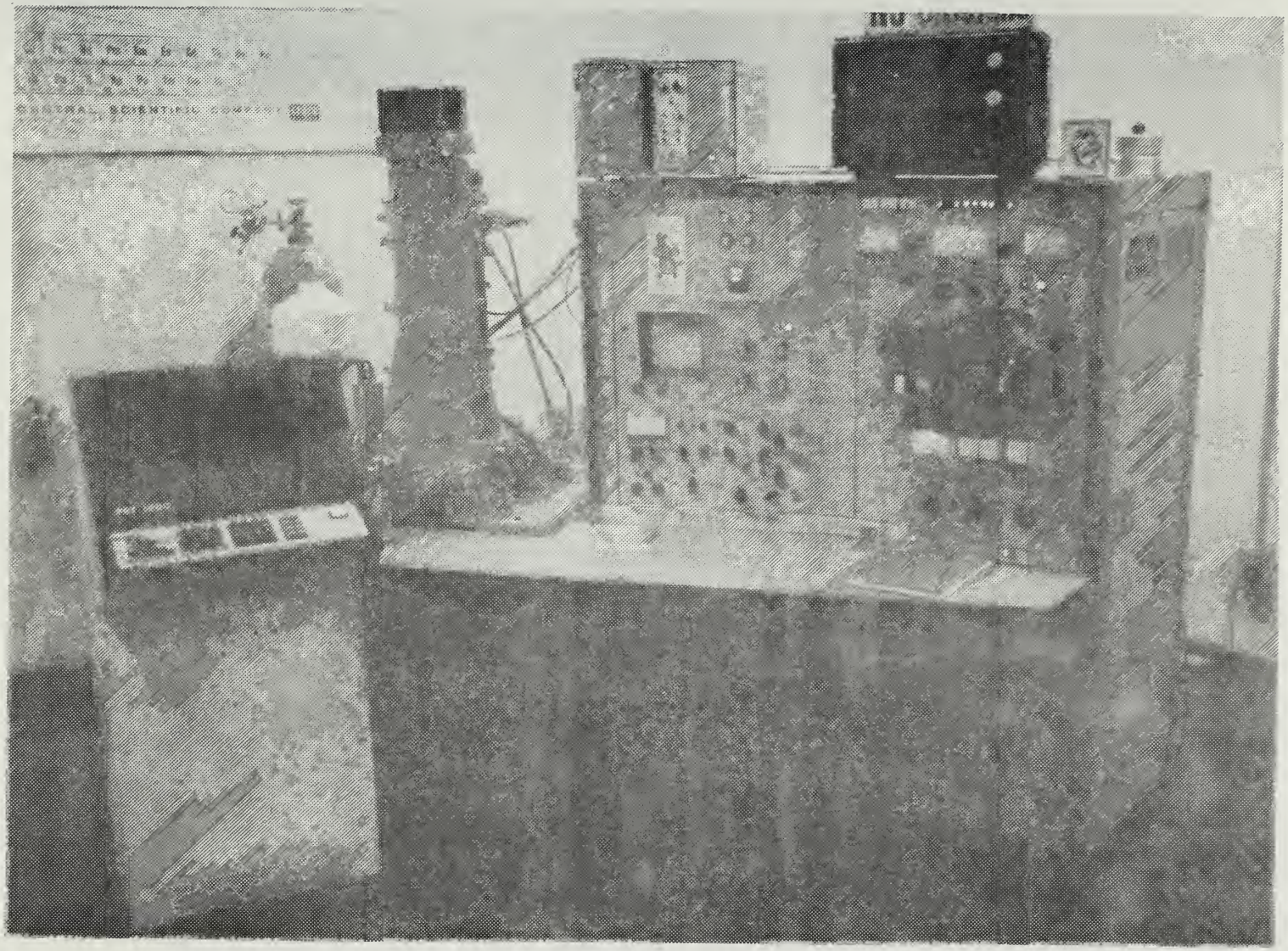

Figure III.E.1 - S4-10 Scanning Electronic Microscope

developed by Professor C. W. Oatley and his colleagues in the Cambridge University Engineering Laboratories. The stereoscan detects and displays information derived from the action of an electron probe scanning the surface of a specimen producing a three-dimensional appearance of the displayed image. The stereoscan has a direct-reading magnification system which provides a useful range between x20 and x100,000 corresponding to scanned areas of 5mm to 2μm square on the specimen. In order that the displayed image can be photographed readily there is a separate display unit provided with a camera mounting. Not only can the topography be examined, but it is also possible to investigate certain electronic characteristics of the specimen. The instrument can be used safely by semi-skilled personnel. The microscope is used in this study to obtain photographs of the fracture surfaces.

IV. ANALYTICAL STUDIES

A. GENERAL CATEGORIES

The analysis of advanced fibrous composites can be broken down into the general categories of Molecular Theory, Micromechanics, Macromechanics, and Structural Analysis, as shown in Figure IV.A.1. Molecular Theory addresses the type and strength of the composite material bonding of the fibers in a polymer matrix. Micromechanics deals with the determination of the properties of a unidirectional fiber reinforced epoxy lamina from the known properties of the basic constituents. This includes fiber-matrix interface stresses, fiber stability, and residual stress distribution. Using the unidirectional lamina or ply as a basic input, Macromechanics considers the determination of angle-plied laminate properties. Structural Analysis of composite structures utilizes existing techniques such as equivalent material substitution, finite elements, anisotropic elasticity, and general energy methods.

B. STRENGTH AND STIFFNESS

Design criteria for composite materials emphasizes the relationship of the performance of the structure to the properties of a ply. A ply is a thin sheet consisting of an oriented array of fibers embeded in a continuous matrix material. These plies, stacked one upon another in a defined sequence and orientation, are bonded together, yielding a

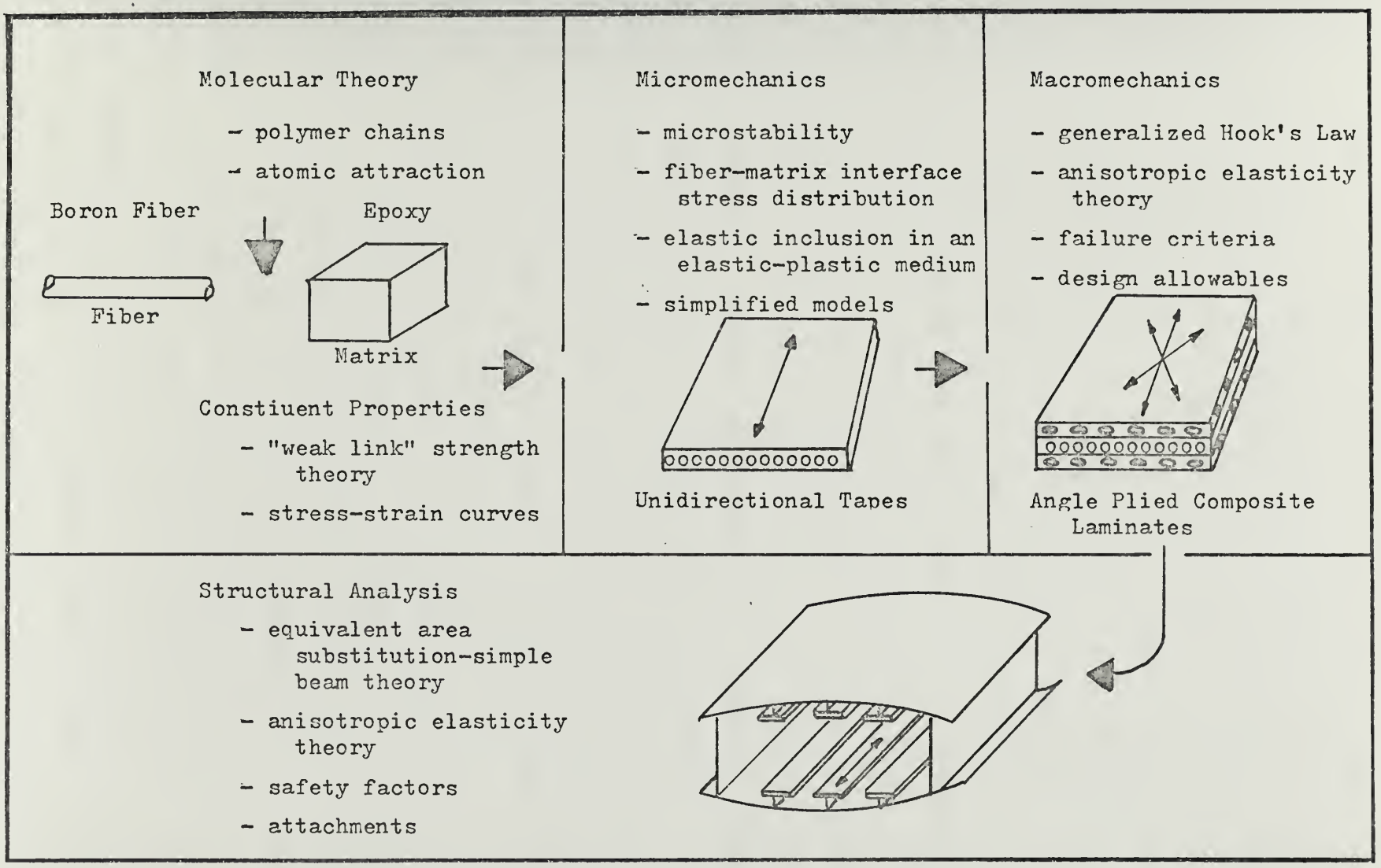

Figure IV.A.1 - Analysis

laminate with tailored properties. The elastic properties of the laminate in a global coordinate system are related to the properties of the individual ply by the specification of the ply thickness, stacking sequence, and the orientation of each ply. The properties of the ply, in turn are specified by the properties of the fiber and the matrix, their volumetric concentration, and the geometric packing in the ply. Generally, the ply material is preformed and can be purchased in a continuous compliant tape or sheet form, which is in a chemically semicured condition. Fabrication of structural items using this "prepreg" material is accomplished by either winding it on a mandrel or cutting and stacking it onto a mold, and then applying heat and pressure to complete the chemical hardening process. Thus, the basis for the engineering design of composite materials is the cured ply as it exists in a laminate. In contrast with isotropic materials, an oriented ply is orthotropic and requires four elastic (plane stress) constants [1] to specify its stiffness properties.

Consider now the general stress-strain behavior of a laminate. Assume the laminate is composed of 7 plies oriented at the angles of 90/+45/-45/0/-45/+45/90 from one surface to the other. This symmetric lay-up is referred to as a balanced design. A definition of balanced design is given in Section IV-C. If an inplane tensile load is applied in the 0-deg fiber direction, the initial slope of the stress-strain curve is related to the sum of the plane-stress stiffness of each ply. As the laminate is deformed, each ply is subjected to

the same inplane strain. When the strain in the 90-deg layers reaches the strain level at which ply failure is experienced, the 90-deg layers crack (craze). In graphite, as well as in glass/resin systems, the occurrence of crazing is associated with an audible noise similar to the creaking of a wooden mast, and a whitening of the material occurs. The failure of the 90-deg ply in the laminate prevents the fibers from carrying their share of the load. This load is transferred to the unbroken layers and results in a loss of laminate stiffness or modulus. Similarly, the 45-deg layers are ultimately strained; failure occurs, transferring all of the load to the 0-deg layers. Continual loading will eventually produce a catastrophic failure of the laminate when the strain capability of the unbroken 0-deg ply is exceeded. Thus, the stress required to craze the system, as well as final failure load, is a function of laminate geometry. Therefore, lamination permits the designer to tailor a fixed prepreg system to meet the conflicting stress/strain demands at different points in a structure.

The properties of a laminate are specified in terms of the ply orientation and orthotropic elastic moduli (E_{11}, E_{22}, ν_{12}, G_{12}), the engineering strains to failure, and the thermal expansion coefficients. Engineering properties of currently commercially available prepreg materials have been tabulated for design references [2].

A study has been conducted to relate specific combinations of ply lay-up angles to the laminate stiffness [3]. In view

of practical considerations, particularly simplicity and achievement of balanced design with a minimum number of plies, the study was limited to only three orientation angles, 0, $\pm\alpha$, $\pm\beta$. In each case, the zero plies represent some fraction of the total number of plies, while the remainder is divided evenly between those at $\pm\alpha$ and $\pm\beta$. The analysis revealed that the maximum stiffness of a laminate is attained when $\alpha = \beta$ and a large proportion of zero plies is used.

C. ENGINEERING PROPERTIES OF FLAT LAMINATES

In the formulation of a linear theory to predict laminate orthotrophic properties from prepreg tape properties, it is assumed that:

(1) transverse normal stress is negligible in the laminate,

(2) there is no relative displacement between the contiguous surface of the plies, and

(3) normals to the midplane of the laminate remain normal.

Development on the basis of these assumptions results in the following relationship between the plate stress resultants N_x, N_y, N_{xy}, M_x, M_y, and M_{xy} and the displacements u, v and w [3]

(IV.C.1)

$$\begin{Bmatrix} N_x \\ N_y \\ N_{xy} \\ M_x \\ M_y \\ M_{xy} \end{Bmatrix} = \begin{bmatrix} \begin{bmatrix} A_{11} & A_{12} & A_{16} \\ A_{12} & A_{22} & A_{26} \\ A_{16} & A_{26} & A_{66} \end{bmatrix} & \begin{bmatrix} B_{11} & B_{12} & B_{16} \\ B_{12} & B_{22} & B_{26} \\ B_{16} & B_{26} & B_{66} \end{bmatrix} \\ \begin{bmatrix} B_{11} & B_{12} & B_{16} \\ B_{12} & B_{22} & B_{26} \\ B_{16} & B_{26} & B_{66} \end{bmatrix} & \begin{bmatrix} D_{11} & D_{12} & D_{16} \\ D_{12} & D_{22} & D_{26} \\ D_{16} & D_{26} & D_{66} \end{bmatrix} \end{bmatrix} \begin{pmatrix} u,_x \\ v,_y \\ u,_y - v,_x \\ w,_{xx} \\ w,_{yy} \\ 2w,_{xy} \end{pmatrix}$$

where

$$A_{ij} = \sum_{k=1}^{n} \bar{Q}_{ij}^{(k)} \quad (h_{k+1} - h_k) \qquad \text{(IV.C.2)}$$

$$B_{ij} = \frac{1}{2}\sum_{k=1}^{n} \bar{Q}_{ij}^{(k)} \quad (h_{k+1}^2 - h_k^2) \qquad \text{(IV.C.3)}$$

$$D_{ij} = \frac{1}{3}\sum_{k=1}^{n} \bar{Q}_{ij}^{(k)} \quad (h_{k+1}^3 - h_k^3) \qquad \text{(IV.C.4)}$$

where the superscript k refers to the ply, and h_k is the distance from the middle plane of the laminate to the top of the k^{th} layer. The reduced stiffness coefficients Q_{ij} can be transformed to the load axis by

(IV.C.5)

$$\bar{Q}_{11} = Q_{11}\cos^4\theta + 2(Q_{12}+2Q_{66})\sin^2\theta\cos^2\theta + Q_{22}\sin^4\theta$$

$$\bar{Q}_{22} = Q_{11}\sin^4\theta + 2(Q_{12}+2Q_{66})\sin^2\theta\cos^2\theta + Q_{22}\cos^4\theta$$

$$\bar{Q}_{12} = (Q_{11}+Q_{22}-4Q_{66})\sin^2\theta\cos^2\theta + Q_{12}(\sin^4\theta + \cos^4\theta)$$

$$\bar{Q}_{66} = (Q_{11}+Q_{22}-2Q_{12}-2Q_{66})\sin^2\theta\cos^2\theta + Q_{66}(\sin^4\theta + \cos^4\theta)$$

$$\bar{Q}_{16} = (Q_{11}-Q_{12}-2Q_{66})\sin\theta\cos^3\theta + (Q_{12}-Q_{22}+2Q_{66})\sin^3\theta\cos\theta$$

$$\bar{Q}_{26} = (Q_{11}-Q_{12}-2Q_{66})\sin^3\theta\cos\theta + (Q_{12}-Q_{22}+2Q_{66})\sin\theta\cos^3\theta$$

where $\bar{Q}_{ij}$ is the transformed reduced stiffness coefficient and Q_{ij} is defined [1,2] as follows:

$$Q_{11} = E_{11} / (1 - \nu_{12}\nu_{21}) \qquad \text{(IV.C.6)}$$

$$Q_{22} = E_{22} / (1 - \nu_{12}\nu_{21}) \qquad \text{(IV.C.7)}$$

$$Q_{12} = \nu_{21}E_{11} / (1 - \nu_{12}\nu_{21}) \qquad \text{(IV.C.8)}$$

$$Q_{66} = G_{12} \qquad \text{(IV.C.9)}$$

$$\frac{\nu_{ij}}{E_{ii}} = \frac{\nu_{ij}}{E_{jj}} \quad (i,j = 1, 2, 6) \qquad \text{(IV.C.10)}$$

where subscripts 1 and 2 refer to the longitudinal and transverse axis of the laminate. The A_{ij} relate the inplane forces to the inplane strains of a laminate and are therefore termed the "extensional constants." The B_{ij} relate the plate curvatures to the inplane forces and the inplane strains to the moments. Finally, the D_{ij} relate the moments to the plate curvatures and are termed the "flexural rigidities."

Examination of Equations IV.C.2 - 4 reveals that if the ply layup is symmetric about the midplane, and if there are an equal number of plus and minus angular plies, then there is no coupling between either the inplane forces and the curvatures or between the moments and the inplane strains.

The inplane forces are a function of inplane strain only, and the moments are related only to the curvatures. There is also thermal balance in that there is no warping when the composite is at a temperature different from the curing temperature. This kind of design is referred to as a balanced design. In the balanced design

$$B_{ij} = A_{16} = A_{26} = 0$$

The composite plates tested in this program used NARMCO 5208/T 300 prepreg graphite tape. The properties of the tape are taken from the Advanced Composite Design Guide [4] as

$$E_{11} = 20.5 \times 10^6 \text{ psi}$$

$$E_{22} = 1.47 \times 10^6 \text{ psi}$$

$$G_{12} = 0.75 \times 10^6 \text{ psi}$$

$$\nu_{12} = 0.30$$

Substituting the engineering properties for the lamina in Equations IV.C.6 - 9 we have

$$Q_{11} = 20.63 \times 10^6 \qquad Q_{12} = 0.44 \times 10^6$$

$$Q_{22} = 1.48 \times 10^6 \qquad Q_{66} = 0.75 \times 10^6$$

Evaluating the 9-ply antisymmetric test laminate with the coordinate system shown in Figure III.A.1, we have from Equation IV.C.5

Layers:	1, 5, 9	2, 6	3, 7	4, 8
Orientation:	0°	$+45^\circ$	-45°	90°
$\bar{Q}_{11}$	20.63×10^6	6.50×10^6	6.50×10^6	1.48×10^6
$\bar{Q}_{22}$	1.48×10^6	6.50×10^6	6.50×10^6	20.63×10^6
$\bar{Q}_{12}$	0.44×10^6	5.00×10^6	5.00×10^6	0.44×10^6
$\bar{Q}_{66}$	0.75×10^6	5.31×10^6	5.31×10^6	0.75×10^6
$\bar{Q}_{16} = \bar{Q}_{26}$	0.00	4.79×10^6	-4.79×10^6	0.00

Substituting into Equations IV.C.2 - 4 respectively, yields the quantities

$A_{11} = 679{,}416$	$B_{11} = -561.465$	$D_{11} = 333.632$
$A_{22} = 536{,}190$	$B_{22} = 1{,}580.556$	$D_{22} = 157.452$
$A_{12} = 166{,}141$	$B_{12} = -509.562$	$D_{12} = 46.185$
$A_{66} = 186{,}759$	$B_{66} = -509.551$	$D_{66} = 53.957$
$A_{16} = A_{26} = 0$	$B_{16} = B_{26} = -535.508$	$D_{16} = D_{26} = 4.005$

From the matrix Equation IV.C.1 it can be shown that

$$\begin{Bmatrix} u,_x \\ v,_y \\ u,_y - v,_x \\ \\ w,_{xx} \\ w,_{yy} \\ 2w,_{xy} \end{Bmatrix} = \begin{bmatrix} \begin{bmatrix} a_{11} & a_{12} & a_{16} \\ a_{12} & a_{22} & a_{26} \\ a_{16} & a_{26} & a_{66} \end{bmatrix} & \begin{bmatrix} b_{11} & b_{12} & b_{16} \\ b_{12} & b_{22} & b_{26} \\ b_{16} & b_{26} & b_{66} \end{bmatrix} \\ \begin{bmatrix} b_{11} & b_{12} & b_{16} \\ b_{12} & b_{22} & b_{26} \\ b_{16} & b_{26} & b_{66} \end{bmatrix} & \begin{bmatrix} d_{11} & d_{12} & d_{16} \\ d_{12} & d_{22} & d_{26} \\ d_{16} & d_{26} & d_{66} \end{bmatrix} \end{bmatrix} \begin{Bmatrix} N_x \\ N_y \\ N_{xy} \\ \\ M_x \\ M_y \\ M_{xy} \end{Bmatrix}$$

Inversion of the coefficient matrix in Equation IV.C.1 yields

$$a_{11} = 1.615 \times 10^{-6} \quad b_{11} = 4.759 \times 10^{-7} \quad d_{11} = 3.150 \times 10^{-3}$$

$$a_{22} = 2.123 \times 10^{-6} \quad b_{22} = -2.511 \times 10^{-5} \quad d_{22} = 6.983 \times 10^{-3}$$

$$a_{12} = -5.196 \times 10^{-7} \quad b_{12} = 5.622 \times 10^{-6} \quad d_{12} = -9.567 \times 10^{-4}$$

$$a_{66} = 5.558 \times 10^{-6} \quad b_{66} = 1.607 \times 10^{-5} \quad d_{66} = 1.933 \times 10^{-2}$$

$$a_{16} = 5.976 \times 10^{-8} \quad b_{16} = 6.168 \times 10^{-6} \quad d_{16} = -4.401 \times 10^{-5}$$

$$a_{26} = -8.745 \times 10^{-9} \quad b_{26} = 1.607 \times 10^{-5} \quad d_{26} = -4.431 \times 10^{-4}$$

Thus, the "effective" Young's modulus and shear modulus of this antisymmetric angular ply test laminate is [2]

$$E_1 = \frac{1}{t\, a_{11}} = 9.198 \times 10^6 \text{ psi}$$

$$E_2 = \frac{1}{t\, a_{22}} = 7.000 \times 10^6 \text{ psi}$$

$$G_{12} = \frac{1}{t\, a_{66}} = 2.673 \times 10^6 \text{ psi}$$

$$\nu_{21} = \frac{-a_{12}}{a_{22}} = 0.245$$

$$\nu_{12} = \frac{-a_{12}}{a_{11}} = 0.322$$

D. NATURAL FREQUENCIES

The recent emergence of composite materials as structural members of aerospace vehicle designs carries with it the desirability of testing each proposed design and fabrication

procedure prior to its general use. Some of the more common flaws found in composites include layer delaminations, cracks, resin rich or resin poor areas, porosity or voids and fiber matrix debonding. Ultrasonic testing, using a vibratory phenomenon, possesses the greatest flexibility for nondestructive testing and evaluation of composite materials and is one of the most popular techniques generally used. It is possible that a similar kind of testing, i. e. measurement of the natural frequencies of the structure, can be used to determine qualitatively the degree of damage of the composite.

The coupled differential equations of the eigenvalue problem for the natural frequencies of antisymmetric angle-ply test laminates [5] are

(IV.D.1 - 3)

$$A_{11}u_{,xx} + A_{66}u_{,yy} + (A_{12} + A_{66})v_{,xy} - 3B_{16}w_{,xyy} - B_{26}w_{,yyy} = 0$$

$$(A_{12} + A_{66})u_{,xy} + A_{66}v_{,xx} + A_{22}v_{,yy} - B_{16}w_{,xxx} - 3B_{26}w_{,xyy} = 0$$

$$D_{11}w_{,xxxx} + 2(D_{12} + 2D_{66})w_{,xxyy} + D_{22}w_{,yyyy} - B_{16}(3u_{,xxy} + v_{,xxx}) - B_{26}(u_{,yyy} + 3v_{,xyy}) - \rho\omega^2 w = 0$$

when the inplane inertia forces are neglected; ρ is the mass per unit area, and ω is the natural frequency. A solution to these equations is sought satisfying the prescribed boundary conditions. This solution furnishes the natural frequencies and their corresponding modes. Methodology in the formal solution of plate vibration equations is contained in [6].

If the plate dimensions are such that the plate can be modeled as a beam, i. e. $u,w \neq f(y)$ and $v = 0$, then Equations IV.D.1 - 3 can be simplified to the simple beam equation

$$D_{11}w,_{xxxx} - \rho\omega^2 w = 0 \qquad \text{(IV.D.4)}$$

The solution to this equation for a cantilever beam is obtained from the transcendental equation [7]

$$\cos \lambda L = -1/\cosh \lambda L$$

where L is the length of the beam, and $\lambda^4 = \rho\omega^2/D_{11}$. For the fundamental frequency

$$\lambda L = 1.876$$

This simplification to a beam is employed in Section V.C where the natural frequencies of damaged and undamaged samples from the composite plates are presented.

V. RESULTS

A. ENGINEERING PROPERTIES

Three standard tensile specimens were made from the graphite/epoxy test plate as described in the Advanced Composite Design Guide [4]. The orientation of each specimen is shown in Figure V.A.1. The principal directions 1 and 2 were chosen parallel and perpendicular to the 0-deg oriented plys of the laminate, respectively. Back-to-back biaxial strain gages were bonded on both sides of each specimen in order to average any tendency toward bending and torsion stresses imposed by the grips of the tensile testing machine and the antisymmetrical design. A uniaxial tension was applied to each specimen, the strains per specimen were measured and averaged, and stress-strain plots were obtained. The results of the test on the first specimen (load applied parallel to the 1-direction) is shown in Figure V.A.2. From this graph the following "effective" properties were calculated.

$$E_1 = \frac{\sigma_1}{\varepsilon_1} \qquad \text{(V.A.1)}$$

$$\nu_{12} = -\frac{\varepsilon_2}{\varepsilon_1} \qquad \text{(V.A.2)}$$

The load on the second specimen was applied parallel to the 2-direction. The results are given in Figure V.A.3. From these results

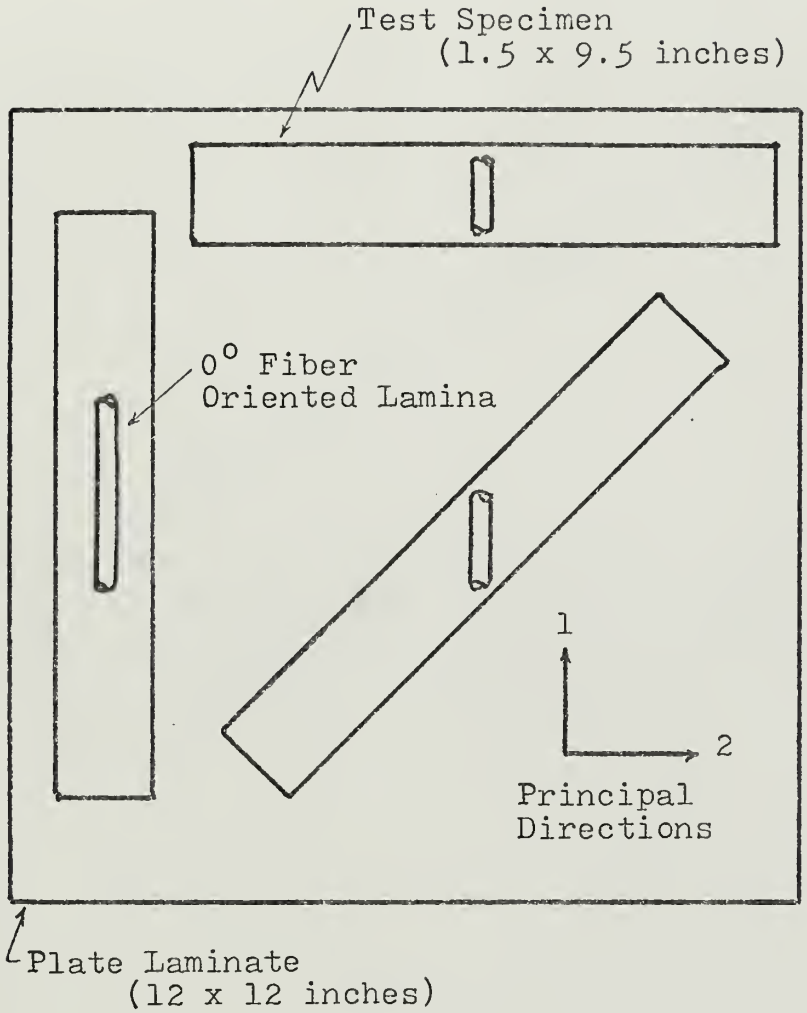

Figure V.A.1 - Tensile Specimen

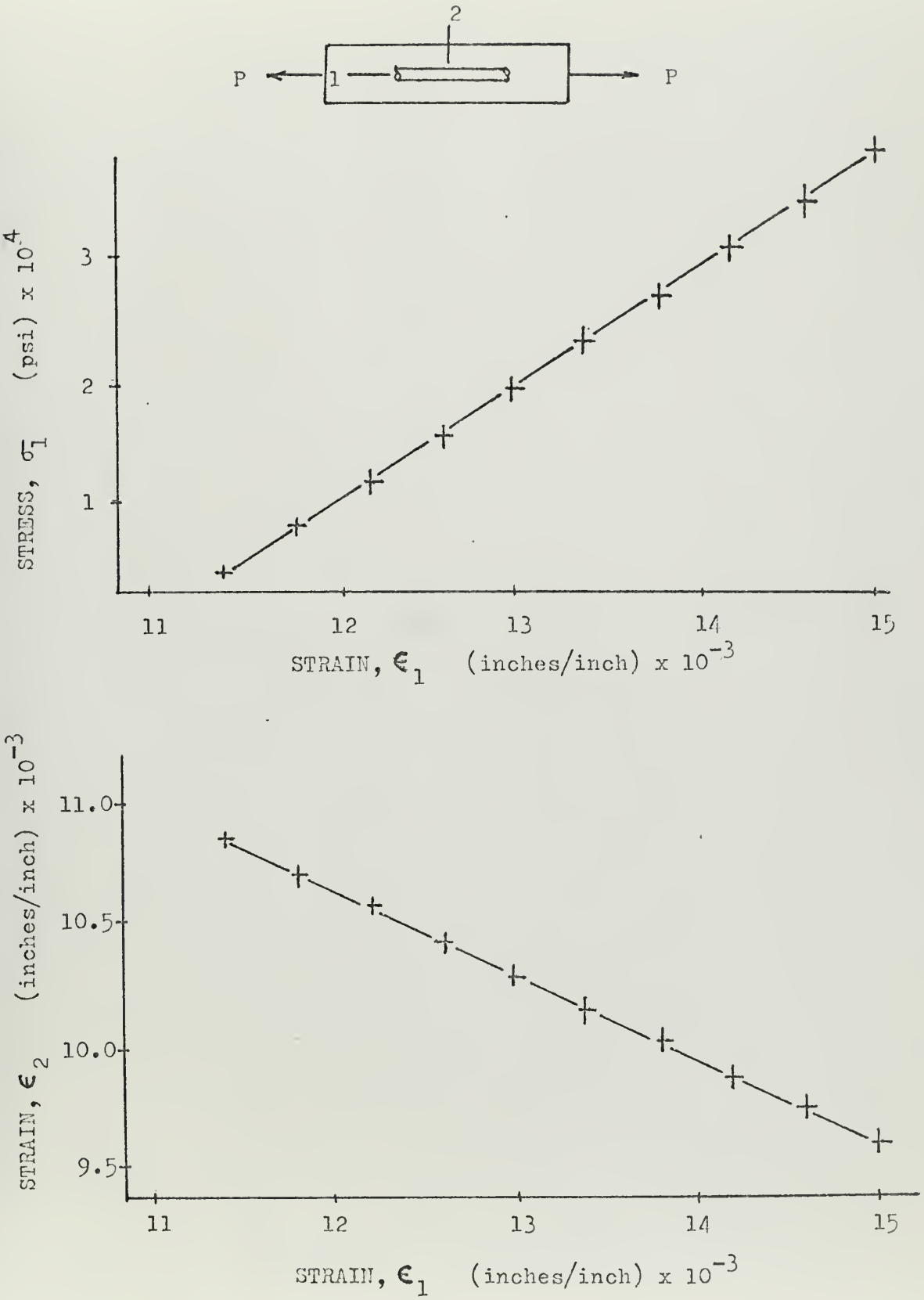

Figure V.A.2 - Stress-Strain Response of First Specimen

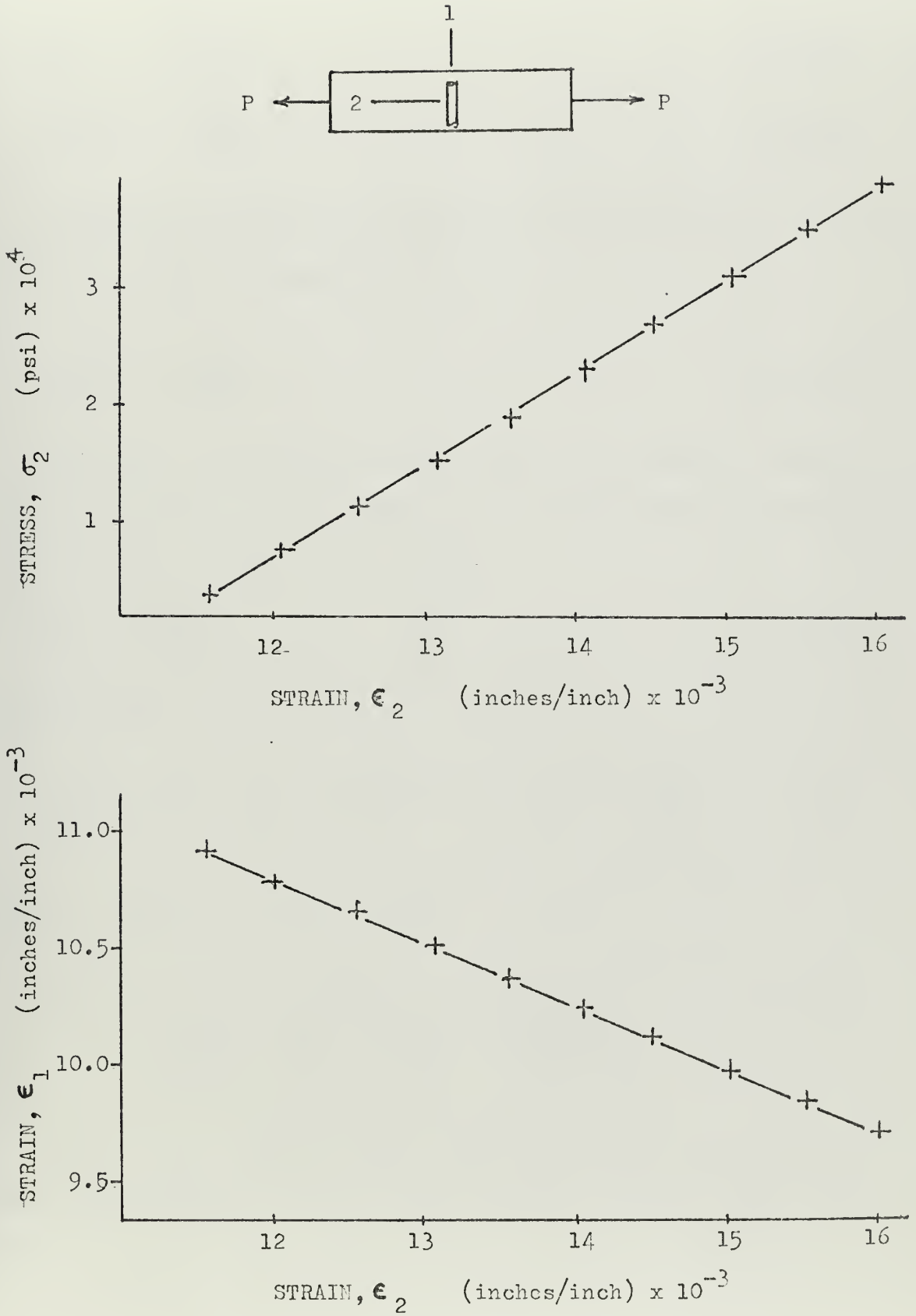

Figure V.A.3 - Stress-Strain Response of Second Specimen

$$E_2 = \frac{\sigma_2}{\varepsilon_2} \qquad \text{(V.A.3)}$$

$$\nu_{21} = -\frac{\varepsilon_1}{\varepsilon_2} \qquad \text{(V.A.4)}$$

Accuracy of these measurements was checked by the reciprocal relations given by Equation IV.C.9

$$\frac{\nu_{12}}{E_1} = \frac{\nu_{21}}{E_2} \qquad \text{(V.A.5)}$$

The final specimen was subjected to a uniaxial tension load at 45-deg to the 1-direction and the data is plotted in Figure V.A.4. This graph yields

$$E_\xi = \frac{\sigma_\xi}{\varepsilon_\xi} \qquad \text{(V.A.6)}$$

where [8]

$$\frac{1}{E_\xi} = \frac{1}{4}\left(\frac{1}{E_1} - \frac{2\nu_{21}}{E_2} + \frac{1}{G_{12}} + \frac{1}{E_2}\right) \qquad \text{(V.A.7)}$$

wherein G_{12} is the only unknown. Thus,

$$G_{12} = \frac{1}{\left(\frac{4}{E_\xi} - \frac{1}{E_1} - \frac{1}{E_2} + \frac{2\nu_{21}}{E_2}\right)} \qquad \text{(V.A.8)}$$

Table V.A.1 contains the "effective" properties based upon the measured data and the computed results from Section IV.C.

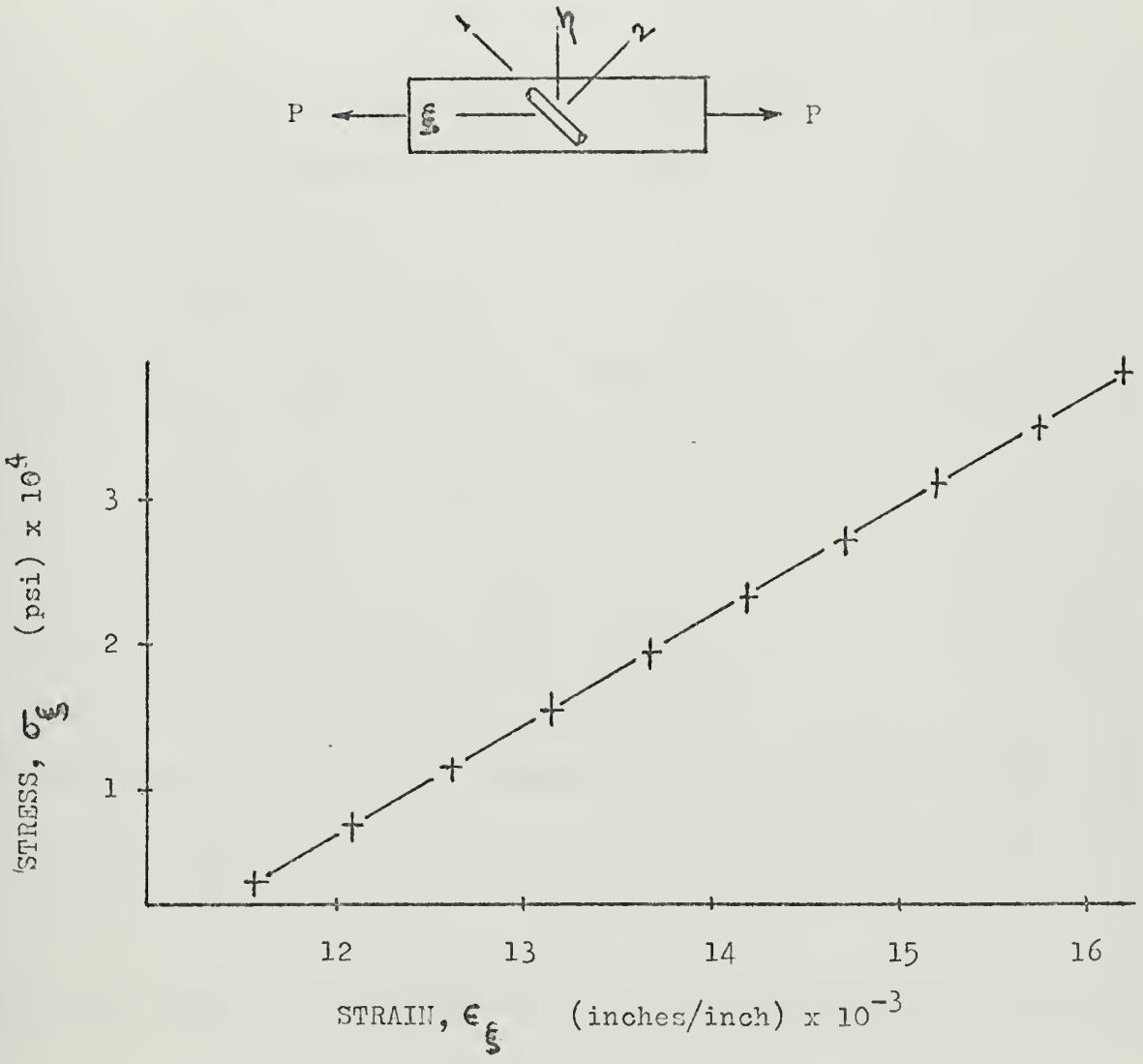

Figure V.A.4 - Stress-Strain Response of Third Specimen

TABLE V.A.1

Analytical/Experimental Comparison
of
Engineering Properties

Properties	Analytical	Experimental	% Error
E_1	9.198×10^6 psi	9.581×10^6 psi	-4.0
E_2	7.000×10^6 psi	7.709×10^6 psi	-9.2
ν_{12}	0.322	0.353	-8.8
ν_{21}	0.245	0.259	-5.4
G_{12}	2.673×10^6 psi	2.573×10^6 psi	+3.8

Reciprocal Relation	Analytical	Experimental
$\frac{\nu_{12}}{E_1} - \frac{\nu_{21}}{E_2} = 0$	$= 0$	$= 3 \times 10^{-3}$

B. BALLISTIC PENETRATION WITH/WITHOUT HYDRAULIC RAM

Eight entry wall specimens were impacted with .222 caliber projectiles at velocities between 2606 to 2784 fps. Seven of the plates were composite and one was a 7075 T6 aluminum plate, 0.050 inches thick. One of the seven composite specimens was tested without the hydraulic ram effect, i.e. no fluid in the tank.

Two damage areas in the composite plates became evident during the testing with hydraulic ram; the impact area about the center of the plate caused by projectile penetration and the area in the vicinity of the clamped edge. Other than the hole due to the projectile penetration, the impact area damage was limited to delamination of the outermost plies of the plate dry face. Surface delamination was evident for as much as 0.50 to 2 inches on each side of the hole. No significant delamination of the plate wet face was observed. Figure V.B.1 shows the impact area damage of both the wet and dry face. The penetration holes in all test plates were essentially the same size as the projectile diameter; approximately 0.25 inches.

In contrast to the limited damage at the impact area, significant damage was observed about the clamped edges of the plate; as shown in Figure V.B.2. Partial plate failure about the test plate outer perimeter was observed at velocities between 2600 to 2650 fps. However, above 2650 fps excessive delamination became predominant, causing laminae

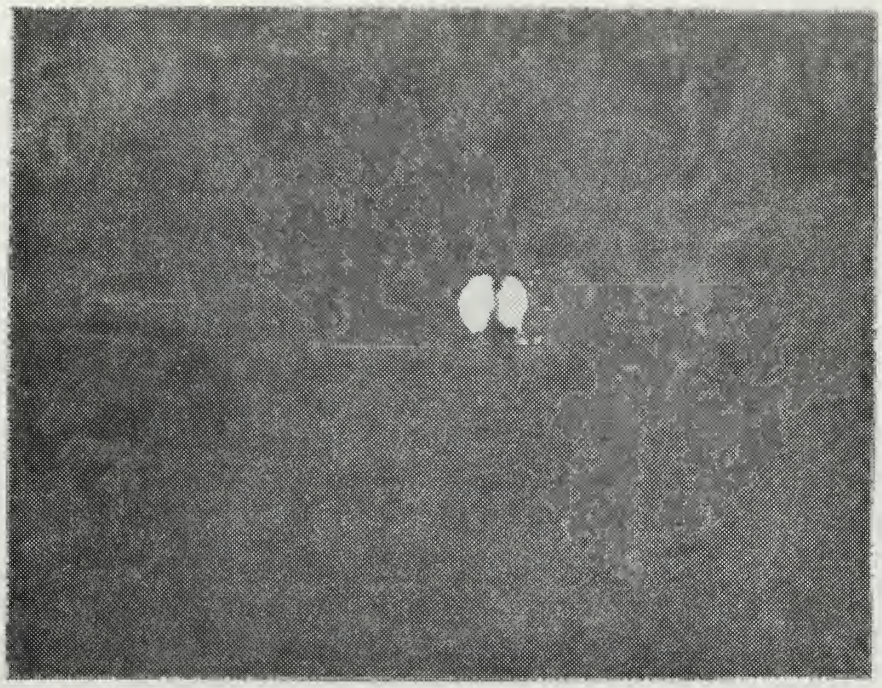

Dry Face

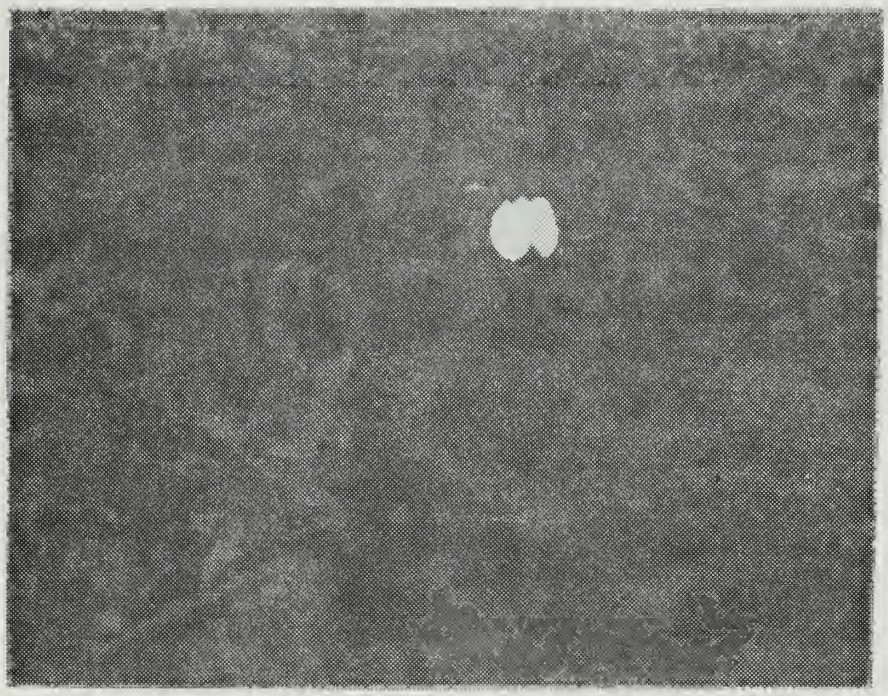

Wet Face

Figure V.B.1 - Impact Damage Area

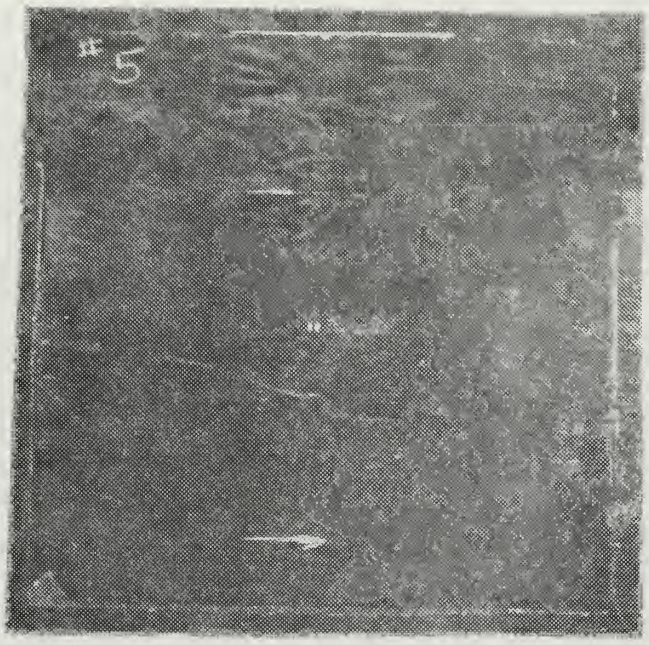

Dry Face

Wet Face

Figure V.B.2 - Clamped Boundary Damage Area

cracks parallel to the fiber direction, and over much of the outer perimeter the laminate was severed from its clamped edge support. The damage along the boundaries also consisted of contiguous area delamination between layers and fibers of the impacted plate.

No damage due to hydraulic ram was observed in the aluminum plate test with a projectile velocity of 2500 fps.

In order to make evident the effects of hydraulic ram, a laminated plate of identical design was subjected to ballistic impact without the fluid in the tank. The damage observed was minimal; a cut-out of diameter the size of the projectile, no significant delamination of the first and second lamina, and no indication of any plate failure at the boundaries.

C. NATURAL FREQUENCIES OF DAMAGED PLATES

Three composite plates and the aluminum plate were used in the vibration test. The conditions of each plate are presented in Table V.C.1.

TABLE V.C.1

Vibration Test Specimens

Plate #	Material	Thickness	Conditions
1A	7075 T6 aluminum	0.050	ballistic penetration @ center with hydraulic ram
4	graphite/epoxy	0.067	ballistic penetration @ center with hydraulic ram
6	graphite/epoxy	0.067	ballistic penetration @ center with no hyrdaulic ram
7	graphite/epoxy	0.067	no ballistic impact

Three test specimens were cut from each plate as shown in Figure V.C.1. Each specimen was positioned between two clamped metal plates as shown in Figure V.C.2. The metal plates were fixed to the shaker. The lowest frequency at which resonance occurred was recorded for each plate specimen. Similarly, frequency measurements were taken with each specimen clamped at the opposite end. The results of these tests are given in Figure V.C.1, where the location of the frequency denotes the clamped end. The predicted frequency for the undamaged specimen from Equation IV.D.4 is also given in Figure V.C.1.

When comparing the frequency of the center strip to that of the end strips of each plate tested, the following was observed: no significant frequency deviation of the aluminum plate (ballistic penetration with hydraulic ram) and the undamaged composite laminate (no ballistic impact); a 6-7 percent frequency decrease of the composite laminate subjected to ballistic penetration (no hydraulic ram); a 9 percent frequency increase of the composite laminate with both ballistic penetration and ram effect. Visual examination of the last laminate indicated probable delamination of the end strips caused by the clamped edge boundary damage.

The bending stiffness of the composite laminate (D_{11}) is equivalent to the bending stiffness of the aluminum plate ($Et^3/12(1-\nu^2)$) when comparing cantilever beam natural

Location of Plate Specimens

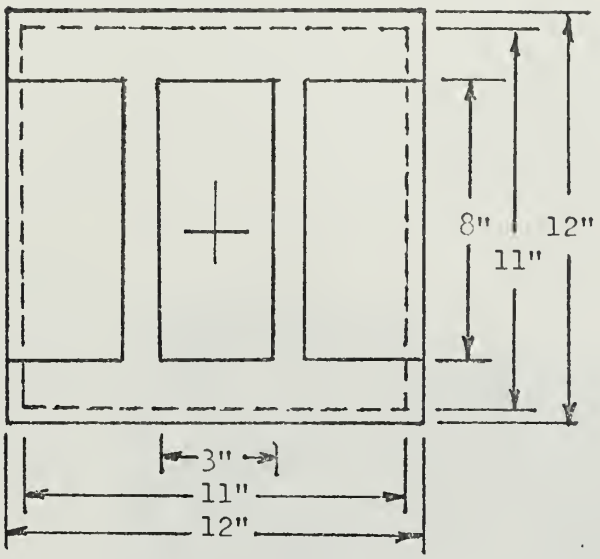

Plate # 1 A

22.7 cps 22.5 cps 22.7 cps

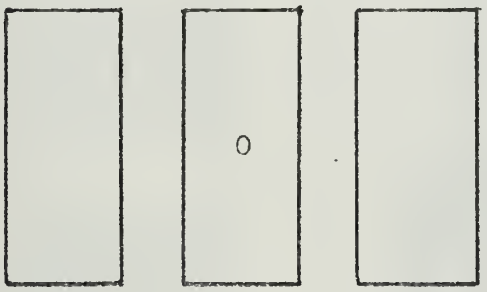

22.7 22.5 22.7

ω = 25.1

Plate # 4

36.6 cps 40.6 cps 36.5 cps

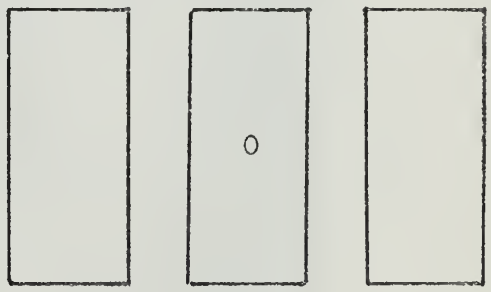

35.0 37.4 34.9

ω = 47.5

Plate # 6

37.1 cps 34.6 cps 36.9 cps

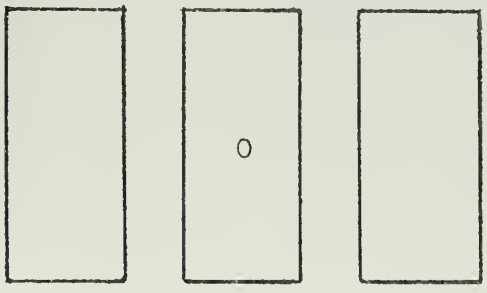

37.5 35.2 38.0

ω = 47.5

Plate # 7

36.9 cps 38.2 cps 38.1 cps

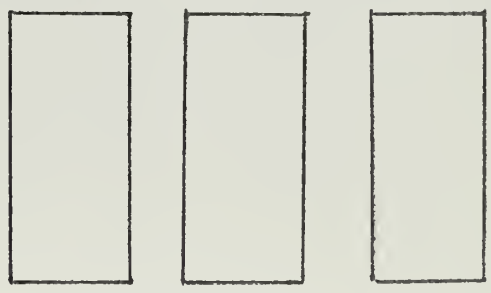

36.9 36.2 35.6

ω = 47.5

Figure V.C.1 - Plate Vibration Test Specimens

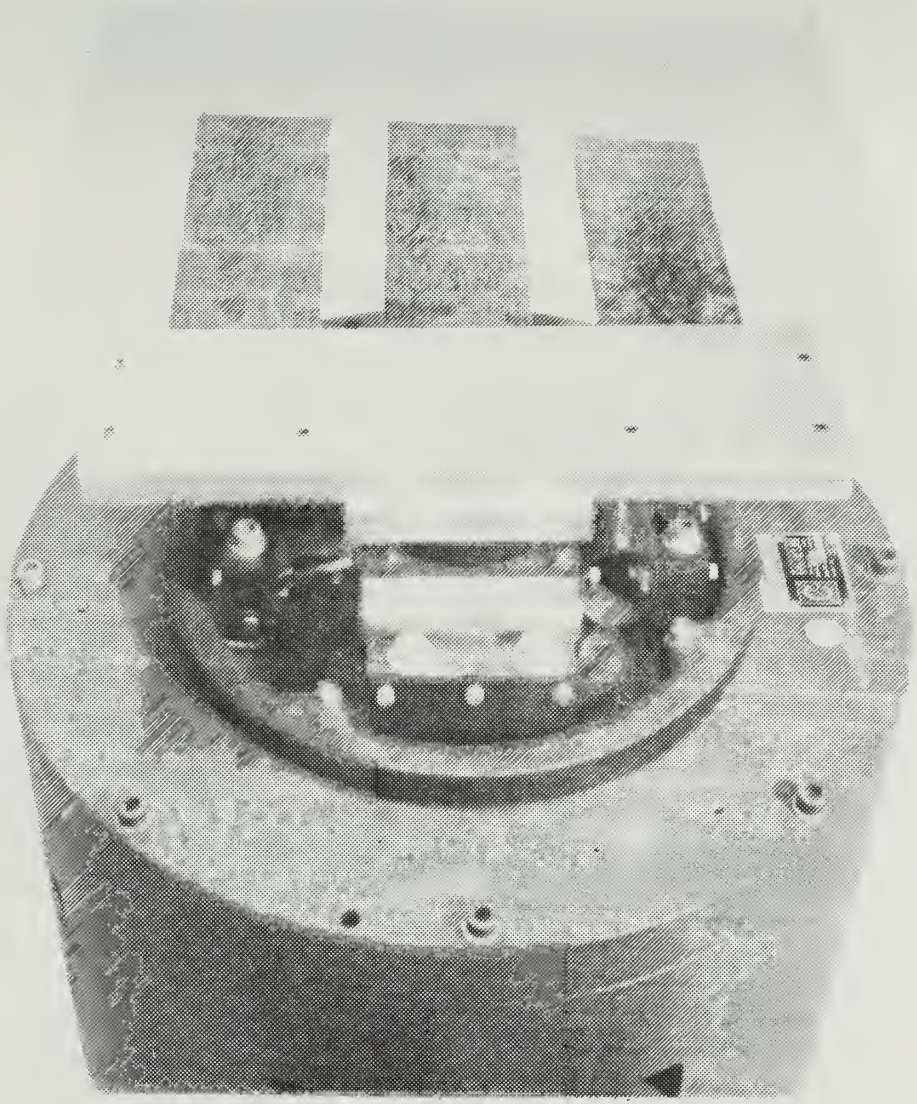

Figure V.C.2 - Specimen Positioning @ Shaker

frequencies. This comparison revealed that the composite plate is approximately three times stiffer, 29 percent lighter, and has a fundamental frequency 63 percent higher than the aluminum plate.

VI. DISCUSSION AND CONCLUSION

A comparison of the effective material properties of the test laminate obtained analytically from the generalized Hooke's Law, and experimentally with use of the biaxial strain gages, is shown in Table V.A.1. In general the agreement is good. A key parameter in the experimental results is the imposition of a uniform stress or strain state in the specimens. Such a loading is relatively easy to obtain in isotropic materials. However, the orthotropicity of composites introduces coupling between the stresses and the strains when loaded in nonprincipal material directions. The validity of the experimental results is reflected by concurrence of the reciprocal relations (Equation V.A.5) in Table V.A.1.

Other possible causes of disagreement between the theoretical and the experimental material properties may be attributed to the varied behavior of the matrix resin from that of the resin within a lamina, inadequate curing of the laminates, and inelastic residual thermal strains in the resin caused by high temperature lamina fabrication.

The damage to the composite plates with hydraulic ram occurred in the impact area and along the outer perimeter. At the impact area, brittle fracture occurred (Figure VI.1) with significantly less delamination beyond the first and second laminae. However, the localized damage about the impact area is relatively insignificant when compared to the catastrophic

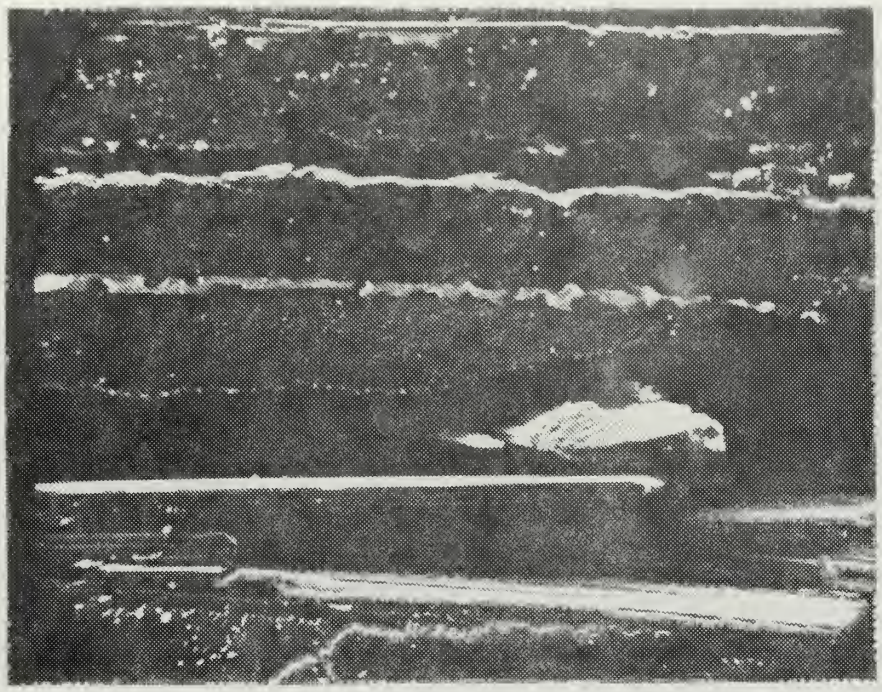

DELAMINATION
Magnification 50x

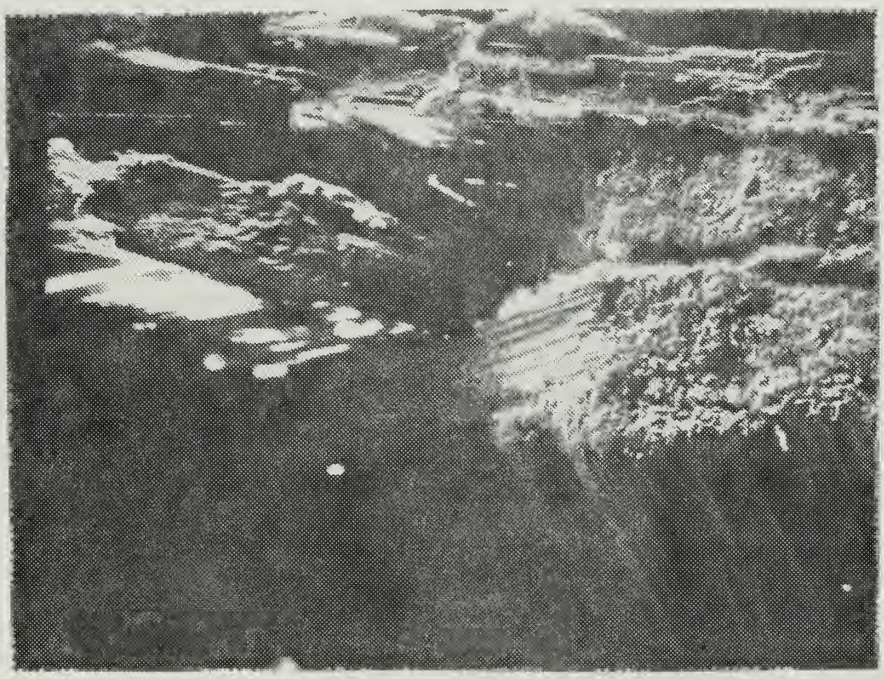

FRACTURE
Magnification 50x

Figure VI.1 - Microscopic Plate Damage

severence at the clamped boundaries of the laminate at the higher projectile velocities. This type of failure may be attributed to the combined effect of entry wall bending and stretching produced by the hydraulic ram and restricted plate flexibility due to the limited slope and displacement at the clamped boundaries. This restriction causes large bending and inplane strains, and hence stresses, at the plate boundary. When any material limit is exceeded there, damage will occur.

As observed from the relative damage between the composite plates and the aluminum plate, the strength of the graphite/epoxy laminate is significantly less than that of the aluminum under this type of loading, support condition and plate dimensions. The strength of the composite plate is affected by the manufacturing process. Since the composite plates had visible delamination prior to testing, the strength of these plates was probably lower than expected.

The measured fundamental frequencies of the undamaged composite specimens were found to be lower than those predicted. This difference is probably due to the delaminated condition of the plate, to the fact that the matrix was thicker than normal causing the plate to measure thicker than it actually should have been, and to the visual difficulties in determining a resonance condition. The relationship between the natural frequency and the extent of composite plate damage was observed to be influenced by the amount of damage along the edge caused by the hydraulic ram.

In conclusion, survivability is an important aspect of aircraft structural design and any proposed new structure should be at least as survivable as the one which it replaces. It is therefore evident from the results of this research that a designer must devote special attention to the capability of composite aircraft fuel cell walls to withstand hydraulic ram, and, in particular, to the type of boundary attachments.

VII. RECOMMENDATIONS

An analytical and experimental hydraulic ram program has been conducted at the Naval Postgraduate School for approximately three years. The study has now been augmented to include advanced fibrous reinforced composites. Although numerous research areas are apparent, a few specific recommendations are in order.

Macroscopic examination of the test plates used indicate that manufacturing and curing processes must be properly carried out to assure the design strength and stiffness of the laminates.

The compatibility problem of graphite with a matrix system needs to be studied.

The number of plies, ply orientation, mass of projectile, angle and velocity at impact, plate boundary conditions, distance between boundaries, effect of supports, size of test fuel cell and amount of liquid are some of the variables which influence test data. Information reflecting the degree of influence of each of these variables would be a major contribution towards understanding the effects of hydraulic ram on composites.

As illustrated by this research, one damage mechanism of the composite plates is delamination between the plies. Perhaps the surface characteristics of the laminae, which control the delamination process, may be changed to increase the ability of the laminate to absorb energy without delaminating.

The use of non-destructive test methods such as ultrasonics, radiography, X-rays, dye penetrates, photoelasticity and holography to estimate laminate damage should be investigated.

Finally, the results presented here vividly illustrate the importance of the method of attachment of the laminate at its boundaries. Thus, studies should be conducted on representative aircraft fuel cell composite joint designs to determine their ability to withstand hydraulic ram.

LIST OF REFERENCES

1. Ashton, J. E., Halpin, J. C., and Petit, P.H., Primer on Composite Material: Analysis, Technomic Publishing Company, Inc., 1969.

2. Structural Design Guide for Advanced Composite Application, Vol. II, North American Rockwell Corporation, 1971.

3. McQuillen, E. J., and Huang, S. L., Graphite-Epoxy Wing for BQM-34E Supersonic Aerial Target, American Institute of Aeronautics and Astronautics, June 1971.

4. Advanced Composite Design Guide, Vol. IV, Rockwell International Corporation, 1973.

5. Jones, R. M., Mechanics of Composite Materials, McGraw-Hill Book Company, 1975.

6. Timoshenko, S. P., Vibration Problems in Engineering, Van Nostrand, 1954.

7. Rogers, G. L., Dynamics of Framed Structures, John Wiley & Sons, Inc., 1959.

8. Calcote, L. R., The Analysis of Laminated Composite Structures, Van Nostrand Reinhold Company, 1969.

9. Foreign Object Impact Damage to Composites, ASTM STP 568, American Society for Testing and Materials, 1975.

10. Analysis of the Test Methods for High Modulus Fibers and Composites, ASTM STP 521, American Society for Testing and Materials, 1972.

11. Applications of Composite Materials, ASTM STP 524, American Society for Testing and Materials, 1972.

12. Power, H. L., FY 74 Experimental Hydraulic Ram Studies, NPS-57Ph74081, August 1974.

13. Soper, W. R., Hydraulic Ram Studies, M. S. Thesis, Naval Postgraduate School, Monterey, 1973.

INITIAL DISTRIBUTION LIST

		No. Copies
1.	Defense Documentation Center Cameron Station Alexandria, Virginia 22314	2
2.	Library, Code 0212 Naval Postgraduate School Monterey, California 93940	2
3.	Department Chairman, Code 57 Department of Aeronautics Naval Postgraduate School Monterey, California 93940	2
4.	Dr. R. E. Ball, Code 57Bp Department of Aeronautics Naval Postgraduate School Monterey, California 93940	2
5.	Dr. M. H. Bank, Code 57Bt Department of Aeronautics Naval Postgraduate School Monterey, California 93940	1
6.	LCDR A. N. Duva, Jr. 205 Vernon Avenue Paterson, New Jersey 07503	1